Systematic analysis of RhoGEF/GAP localizations uncovers regulators of mechanosensing and junction formation during epithelial cell division

Florencia Di Pietro, Mariana Osswald, José M de las Heras, Inês Cristo, Jesús López-Gay, Zhimin Wang, Stéphane Pelletier, Isabelle Gaugué, Adrien Leroy, Charlotte Martin, et al.

Article

Current Biology

Systematic analysis of RhoGEF/GAP localizations uncovers regulators of mechanosensing and junction formation during epithelial cell division

Graphical abstract

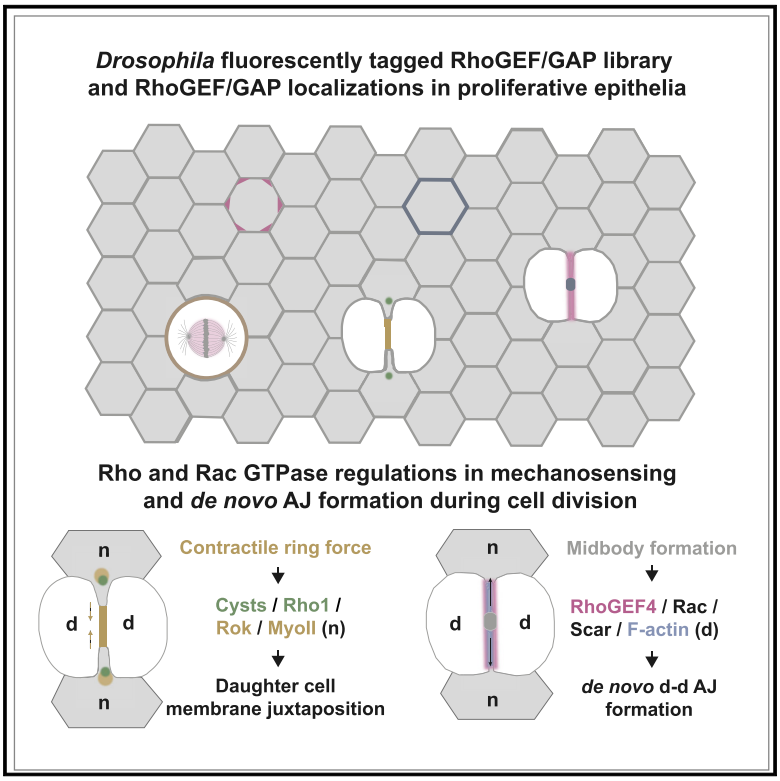

Authors

Florencia di Pietro, Mariana Osswald, José M. De las Heras, ..., Charlotte Martin, Eurico Morais-de-Sá, Yohanns Bellaïche

Correspondence

eurico.sa@ibmc.up.pt (E.M.-d.-S.), yohanns.bellaiche@curie.fr (Y.B.)

In brief

di Pietro et al. generated the complete *Drosophila* library of endogenously tagged RhoGEF/GAPs for a systematic spatiotemporal characterization of RhoGTPase regulation in epithelia. This led to the discovery that Cysts and RhoGEF4 play sequential roles in mechanosensing and junction dynamics to couple cytokinesis with junction formation.

Highlights

- Generation of a complete fluorescent transgenic RhoGEF/GAP library in *Drosophila*
- Identification of the intricated RhoGEF/GAP dynamics during epithelial cell division
- Cysts via Rho participates in the neighbor mechanical response to ring contraction
- RhoGEF4 via Rac controls *de novo* junction length and cell packing upon cytokinesis

di Pietro et al., 2023, Current Biology *33*, 858–874
March 13, 2023
https://doi.org/10.1016/j.cub.2023.01.028

CellPress

CellPress
OPEN ACCESS

Current Biology

Article

Systematic analysis of RhoGEF/GAP localizations uncovers regulators of mechanosensing and junction formation during epithelial cell division

Florencia di Pietro,[1,3] Mariana Osswald,[2,3] José M. De las Heras,[1,4] Inês Cristo,[1,4,5] Jesús López-Gay,[1] Zhimin Wang,[1] Stéphane Pelletier,[1] Isabelle Gaugué,[1] Adrien Leroy,[1] Charlotte Martin,[1] Eurico Morais-de-Sá,[2,6,*] and Yohanns Bellaïche[1,5,7,8,*]

[1]Institut Curie, Université PSL, Sorbonne Université, CNRS UMR3215, INSERM U934, Genetics and Developmental Biology, 75005 Paris, France
[2]IBMC - Instituto de Biologia Molecular e Celular; i3S - Instituto de Investigação e Inovação em Saúde, Universidade do Porto, 4200-135 Porto, Portugal
[3]These authors contributed equally
[4]These authors contributed equally
[5]Present address: Cardiac Regeneration and Disease Unit, Centro Cardiovascular da Universidade de Lisboa (CCUL@RISE), Faculdade de Medicina, Universidade de Lisboa, 1649-028 Lisboa, Portugal
[6]Twitter: @Polarity_i3S
[7]Twitter: @bellaiche_y
[8]Lead contact
*Correspondence: eurico.sa@ibmc.up.pt (E.M.-d.-S.), yohanns.bellaiche@curie.fr (Y.B.)
https://doi.org/10.1016/j.cub.2023.01.028

SUMMARY

Cell proliferation is central to epithelial tissue development, repair, and homeostasis. During cell division, small RhoGTPases control both actomyosin dynamics and cell-cell junction remodeling to faithfully segregate the genome while maintaining tissue polarity and integrity. To decipher the mechanisms of RhoGTPase spatiotemporal regulation during epithelial cell division, we generated a transgenic fluorescently tagged library for the 48 *Drosophila* Rho guanine exchange factors (RhoGEFs) and GTPase-activating proteins (GAPs), and we systematically characterized their endogenous distributions by time-lapse microscopy. Therefore, we unveiled candidate regulators of the interplay between actomyosin and junctional dynamics during epithelial cell division. Building on these findings, we established that the conserved RhoGEF Cysts and RhoGEF4 play sequential and distinct roles to couple cytokinesis with *de novo* junction formation. During ring contraction, Cysts via Rho1 participates in the neighbor mechanosensing response, promoting daughter-daughter cell membrane juxtaposition in preparation to *de novo* junction formation. Subsequently and upon midbody formation, RhoGEF4 via Rac acts in the dividing cell to ensure the withdrawal of the neighboring cell membranes, thus controlling *de novo* junction length and cell-cell arrangements upon cytokinesis. Altogether, our findings delineate how the RhoGTPases Rho and Rac are locally and temporally activated during epithelial cytokinesis, highlighting the RhoGEF/GAP library as a key resource to understand the broad range of biological processes regulated by RhoGTPases.

INTRODUCTION

In animal cells, cell division entails drastic cell shape changes necessary for the faithful segregation of the duplicated genome into the two daughter cells. These morphological changes include cell rounding required for correct spindle formation and orientation, as well as cytokinesis to separate the cytoplasms of the daughter cells.[1,2] Studies on single cells and tissues have shown that these cell shape changes are powered by small RhoGTPases that remodel the actomyosin cytoskeleton.[1–3] Moreover, in multicellular contexts, RhoGTPases are also critical to couple cell shape changes and junction dynamics to control tissue polarity, cohesion, and architecture.[4–7] Notably, cell division is tightly linked to cell fate specification as well as tissue growth, morphogenesis, and mechanics.[8–10] Therefore, characterizing the regulation of RhoGTPases and its implication in cytoskeleton and junction dynamics during cell division in tissues is central to understand how cell number and genome integrity are controlled and how tissue architecture and function are established and maintained.

The small RhoGTPases Rho, Rac, and Cdc42 are key pleiotropic regulators of the actomyosin cytoskeleton and cell junction dynamics.[4–7,11,12] They switch between an active GTP-bound state that binds downstream effectors and an inactive GDP-bound state. These states are primarily regulated by Rho guanine exchange factors (RhoGEFs) that activate RhoGTPases by exchanging GDP for GTP and by RhoGTPase-activating factors (RhoGAPs) that promote GTP hydrolysis to GDP, thereby

inactivating RhoGTPases.[13] Individual RhoGEF/GAPs associated with the regulation of cell shape changes, cell division, migration, and polarity have been identified in cultured cells[4,14–19] and, to a lesser extent, by targeted RNAi or mutant analyses in multicellular contexts.[20–25] In addition, by ectopically expressing all human RhoGEF/GAPs in cultured cell lines, a recent study has defined their localizations and biochemical interactomes, enabling a better understanding of single-cell migration.[16,26] Therefore, the mechanisms mediating the spatiotemporal activation of small RhoGTPases are best understood in individual cells in interphase. However, the spatiotemporal regulation of RhoGTPases remains far less explored during cell division or in tissues, impeding our understanding of actomyosin and junction dynamics during interphase and cell division in epithelial tissues.

During animal cell cytokinesis, RhoGTPases control the pronounced cell deformations associated with cytokinetic ring constriction.[1] Numerous studies have converged to show that the assembly and constriction of the actomyosin cytokinetic ring is powered by the membrane redistribution of the RhoGEF ECT2 (*Drosophila* pebble, Pbl) and RacGAP1 (*Drosophila* tumbleweed, Tum) within the dividing cell.[1,27–30] Despite these fundamental findings, the role of most RhoGEF/GAPs during cell division remains poorly explored. In addition, in epithelial tissues, several studies have shown that the drastic cytokinesis cell shape changes are coupled with E-cadherin (Ecad) *adherens* junction (AJ) remodeling and *de novo* AJ formation.[31,32] In particular, epithelial cytokinesis shares general features in several vertebrate and invertebrate tissues: (1) *de novo* AJ formation is coordinated with cytokinesis and relies on mechanosensing processes involving the dividing cell and its neighbors, and (2) the arrangement of the newly formed cell junctions is defined in late cytokinesis, and it is proposed to modulate tissue topology and morphogenesis.[31–42] Some of these epithelial cytokinetic features are known to be regulated by the Rho and Rac GTPases,[36,42] but the mechanisms controlling their local and temporal activations remain unknown.

Toward achieving an integrated view of the spatiotemporal regulation of actomyosin and junction dynamics in proliferative epithelia *in vivo*, we assembled a complete library of fluorescently tagged *Drosophila* RhoGEF/GAPs. We then systematically analyzed RhoGEF/GAP localizations from interphase to cell division in two *Drosophila* epithelial tissues by time-lapse microscopy. By doing so, we unraveled a series of putative regulators of epithelial tissue organization, polarity, and dynamics. These results led us to focus on the RhoGEF Cysts and RhoGEF4, and to characterize their respective roles in mechanosensation and AJ formation during epithelial cell division. Altogether, our work advances the understanding of cell division in epithelial tissues and highlights that the RhoGEF/GAP library will be a relevant resource to investigate how actomyosin and junction dynamics are controlled during development, repair, and homeostatic processes.

RESULTS

Generation of a library of tagged RhoGEF/GAPs and characterization of their localizations in interphasic epithelial cells

Despite the critical roles of RhoGTPases in all epithelial tissues, a systematic characterization of all RhoGEF/GAP localizations has not been performed in any tissue *in vivo*. To enable the systematic exploration of RhoGEF/GAP localizations, we assembled a complete library of *Drosophila* fluorescently tagged RhoGEF/GAPs (26 RhoGEFs, 22 RhoGAPs, see Methods S1A and S1B for tag positions and human orthologs). We first generated bacterial artificial chromosome (BAC) transgenic lines for 9 GFP-tagged RhoGEF/GAPs. The advent of CRISPR-Cas9 methods led us to switch to tagging by CRISPR-Cas9-mediated homologous recombination. We thus produced GFP- or mKate2-tagged insertions for the remaining 39 RhoGEF/GAPs (Figure S1A). Among the generated CRISPR-Cas9-tagged lines, 34 out of the 39 (~87%) tagged alleles were homozygous viable. We also built a plasmid library of homologous recombination donors and guide RNA-expressing vectors to readily edit each RhoGEF/GAP locus to create loss-of-function alleles and then facilitate structure-function analyses or add any other tags for live-imaging or biochemical studies (Figure S1B; Methods S1C and S1D).

As most of the *Drosophila* RhoGEF/GAP localizations have not yet been assessed in polarized epithelial cells *in vivo*, we performed a detailed characterization of all RhoGEF/GAP localizations in interphase in epithelial tissues (Figures S1 and S2; Data S1 and website). This was performed in two distinct tissues characterized by different structural organization and mechanical properties:[43–47] the dorsal thorax epithelium (notum) of the pupa (Figure S1C) and the follicular epithelium (FE) of the adult ovary during their proliferative stages (Figure S1D). In the notum, 43 out of the 48 RhoGEF/GAPs showed detectable accumulations, whereas 30 out of 48 were detected in the FE (Data S1). This systematic assessment of 48 RhoGEF/GAPs confirmed the interphase localization of Cysts (Figures S1E and S1F), RhoGEF2 (Figures S1E and S1F), RhoGAP71E (Figure S1E), Spg (Figure S1E), RhoGEF64C (website), Conu (Figures S1E and S1F), RhoGAP19D (Figures S1G and S1H), RtGEF (Figure S1I), Pbl (Figure S1J), and Tum (Figures S1J and S1K) observed in diverse *Drosophila* epithelial tissues.[20–22,24,25,48–52] In addition, our screen uncovered numerous additional RhoGEF/GAP localizations in each tissue (Figures S2A and S2B; Data S1, website). Interestingly, these localizations might be associated with (1) the regulation of apico-basal polarity or actomyosin dynamics at the junctional, medio-apical, or basal cortex, as exemplified by the distinct localizations observed for Graf (Figures S2C and S2D), CdGAPr (Figures S2C and S2G), RhoGAP1A (Figures S2C and S2G), GEFMeso (Figure S2E), Sos (Figure S2E), Ziz (Figure S2D), Zir (Figure S2D), CG46491 (Figure S2D), RhoGAP15B (Figure S2G), Cdep (Figures S2F and S2H), and RhoGAP5A (Figure S2H); (2) vertex organization or cell rearrangements (Mbc, RhoGAP5A, and Cdep) (Figures S2F and S2H–S2J); and (3) nucleus-related functions (RhoGAP54D, CG43102, CdGAPr, and RhoGEF4) (Figures S2K and S2L). Together, this initial characterization validated the fluorescently tagged library to explore the localizations of RhoGEF/GAPs. We thus next explored the localizations of RhoGEF/GAPs during epithelial cell division.

Deciphering RhoGEF/GAP distributions during epithelial cell division

Epithelial cell division is characterized by a set of cell shape changes necessary to segregate the duplicated genome in the

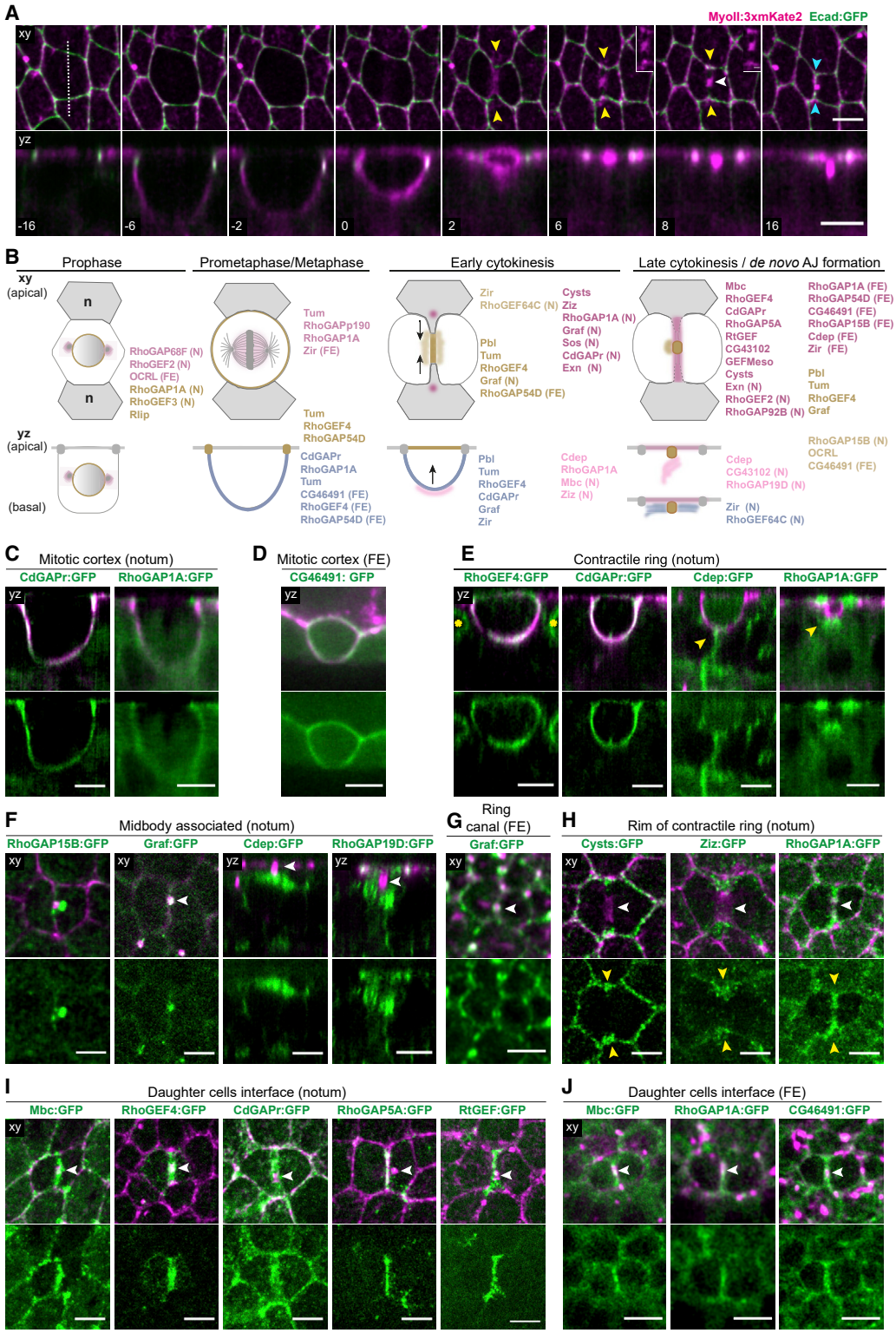

Figure 1. Localizations of RhoGEF/GAPs during epithelial cell division

For all images, "xy" indicates apical confocal top view at the level of the AJ in the notum and FE, while "yz" denotes apical-basal confocal section at the level of the cytokinetic ring or the midbody for the notum or a midsagittal section for the egg chamber. MyoII:3xmKate2 is shown in magenta.

(A) xy (top) and yz (bottom) time-lapse images of Ecad:GFP and MyoII:3xmKate2 during cell division in the notum. Time (min) is set to 0 at the onset of cytokinesis marked by the initial deformation of AJ by the constriction of the cytokinetic ring. Cytokinetic furrowing occurs asymmetrically positioning the midbody apically (from t = 0 to t = 6 min). Upon midbody formation (t = 6 min), a new AJ is formed between the two daughter cells (from t = 6 to t = 16 min). Yellow arrowheads, MyoII

(legend continued on next page)

two daughter cells and by *de novo* AJ formation needed for the maintenance of epithelial organization[1,3,31,32] (Figure 1A). Analyzing MyoII dynamics is instrumental to investigate both cell shape changes and AJ dynamics during cell division.[31,32,53] We therefore systematically analyzed the localization of each RhoGEF/GAP in conjunction with MyoII:3xmKate2 during cell division in the notum and the FE. This analysis confirmed the well-known localization of Pbl and Tum during mitosis and cytokinesis[27–30] (Figures S3A and S3B). It further revealed a complex choreography of RhoGEF/GAP dynamics from prophase to cytokinesis and *de novo* junction formation (Figure 1B; Data S1, website), including sets of RhoGEF/GAPs accumulating around the nuclear envelope during prophase, or labeling the spindle or the centrosomes during cell division (Figures 1B, S3C, S3D, and S3E). Here, we specifically describe cortical and junctional RhoGEF/GAPs for which the subcellular distributions could be associated with cell shape changes or *de novo* junction formation during cell division (Figures 1C–1J and S3F–S3N; Video S1).

RhoGEF/GAP localizations associated with cell shape changes during mitosis

Entry into mitosis is accompanied by cell rounding and a reorganization of actomyosin and junction complexes along the apical-basal axis of epithelial cells.[3,53–55] We found that mitotic entry concurs with significant redistributions of several RhoGEFs and GAPs. In particular, we observed that RhoGEF4 and RhoGAP54D redistributed from the nucleus to the cortex in both tissues (Figure S3F). In parallel, and mirroring the dynamics of MyoII (Figure 1A), several RhoGEF/GAPs expand along the basolateral cortex. This includes CdGAPr and RhoGAP1A in both tissues (Figure 1C) and CG46491 in the FE (Figure 1D). During cell elongation in anaphase, a subset of RhoGEF/GAPs was enriched or depleted from the cell poles in the FE: Mbc accumulated at the cell poles, while the RhoGEF CG46491 was cleared from the cell poles (Figure S3G; Videos S1J and S1L). Together, these RhoGEF/GAPs are good candidates to regulate the actomyosin cytoskeleton or cell junctions during the highly conserved processes of mitotic rounding, anaphase elongation, and polar relaxation.

RhoGEF/GAP localizations associated with ring constriction and midbody formation

In addition to Pbl and Tum that are known to localize at the cytokinetic ring and the midbody,[1,27–30] we identified a large set of RhoGEF/GAPs with distinct localizations during cytokinesis (Figures 1E–1J and S3H–S3N). During early cytokinesis, RhoGEF4 (Figures 1E and S3I), Graf (Figure S3H), CdGAPr (Figures 1E and S3I), and Zir (Figure S3H) localized around the contractile ring. Interestingly, in the notum, we detected several RhoGEF/GAPs localized in a position basal to the cytokinetic ring in previously uncharacterized filamentous or membranous structures. This includes Cdep (Figure 1E; Video S1A), RhoGAP1A (Figure 1E), Mbc (Figure S3H), and Ziz (Figure S3H). Their localization basal to the ring was observed at different time points during ring contraction suggesting distinct functions. Upon completion of ring constriction, another subset of RhoGEF/GAPs was observed associated with the midbody (Figures 1F and S3J), localizing either transiently (RhoGAP15B [Figure 1F], RhoGEF4 [Figure 1I], OCRL [Figure S3J], CG46491, and Mbc [Figure 1J]) or more stably (Graf; Figure 1F) around or at the midbody. Furthermore, we found specific localizations that might be associated with the distinctive midbody dynamics or functions known in each tissue. In the notum, as the midbody moves basally during septate junction formation and abscission,[44,45] we found that Cdep (Figure 1F; Video S1A), RhoGAP19D (Figure 1F), and CG43102 (Figure S3J) accumulated underneath the midbody. In the FE, where abscission is arrested to form ring canals,[56,57] Graf was initially enriched at the midbody and then accumulated on each side of the newly formed ring canal (Figure 1G; Video S1K). Altogether, this group of RhoGEF/GAPs provides entry points to further understand the basic features of epithelial division, such as asymmetric furrowing, midbody dynamics, junction formation, or abscission.

RhoGEF/GAP localizations associated with de novo *AJ formation*

At least two distinct processes couple cytokinesis and *de novo* AJ formation in epithelial tissues.[35,36,38,39,42] The first one is linked to cytokinetic ring contraction, while the second one

accumulation in the neighboring cells during ring constriction; white arrowheads, midbody; cyan arrowheads, new daughter-daughter AJ; inset, close-up on the MyoII signal at the level of the future daughter cell interface.

(B) Schematics of the subcellular localizations of selected RhoGEF/GAPs during epithelial cell division in the notum and the FE in xy (top) and yz (bottom) views. The dividing cell is in white and the neighboring cells (n) are in gray. The RhoGEP/GAP names are color coded according to their localizations in each schematic of the different division phases. Black arrows, direction of cytokinetic furrowing. N or FE indicate localizations exclusively observed in the notum or the FE, respectively. Only RhoGEF/GAPs with a good signal to noise ratio are indicated. See also Data S1 and the website for a complete description.

(C) yz images of CdGAPr:GFP, RhoGAP1A:GFP (top and bottom), and MyoII:3xmKate2 (top) in metaphase cells in the notum.

(D) yz images of CG46491:GFP (top and bottom) and MyoII:3xmKate2 (top) in mitotic cells prior to anaphase in the FE.

(E) yz images of RhoGEF4:GFP, CdGAPr:GFP, Cdep:GFP, RhoGAP1A:GFP (top and bottom), and MyoII:3xmKate2 (top) during cytokinetic ring contraction in the notum. RhoGEF4:GFP is localized at the nuclear envelope membrane in neighboring interphasic cells (yellow asterisks, see also Figure S5A). Yellow arrowheads, Cdep:GFP and RhoGAP1A:GFP enrichments below the cytokinetic ring.

(F) xy images of RhoGAP15B:GFP, Graf:GFP (top and bottom), and MyoII:3mKate2 (top) and yz images of Cdep:GFP, RhoGAP19D:GFP (top and bottom), and MyoII:3xmKate2 (top) during late cytokinesis in the notum. White arrowheads, midbody.

(G) xy images of Graf:GFP (top and bottom) and MyoII:3xmKate2 (top) during ring canal formation in the FE. White arrowhead, ring canal.

(H) xy images of Cysts:GFP, Ziz:GFP, RhoGAP1A:GFP (top and bottom), and MyoII:3xmKate2 (top) during cytokinetic ring constriction in the notum. White arrowheads, cytokinetic ring; yellow arrowheads, Cysts:GFP, Ziz:GFP, and RhoGAP1A:GFP enrichments in the vicinity or at the rim of cytokinetic ring.

(I) xy images of Mbc:GFP, RhoGEF4:GFP, CdGAPr:GFP, RhoGAP5A:GFP, RtGEF:GFP (top and bottom), and MyoII:3xmKate2 (top) during late cytokinesis or *de novo* daughter cell junction formation in the notum. White arrowheads, midbody.

(J) xy images of Mbc:GFP, RhoGAP1A:GFP, CG46491:GFP (top and bottom), and MyoII:3xmKate2 (top) during late cytokinesis or *de novo* daughter cell junction formation in the FE. White arrowheads, midbody.

Scale bar, 5 μm for (A–J) and 1 μm (inset in A).

See also Figures S1–S3, Methods S1A and S1B, Data S1A and S1B, and Video S1.

occurs upon midbody formation. During ring constriction, the dividing and neighboring cell membranes co-ingress, and the contractile force of the ring triggers a mechanosensing process, leading to junctional or actomyosin reorganization at the rim of the apical cytokinetic ring in the neighboring cells.[35,36,42] Upon midbody formation, the second process involves a Rac- and Arp2/3-dependent F-actin accumulation at the midbody and at the prospective daughter cell interface. This promotes the withdrawal of the ingressed neighboring cell membranes and *de novo* daughter-daughter AJ formation.[36,39] We therefore examined RhoGEF/GAP distributions at the rim of the apical cytokinetic ring during its constriction and at the level of the prospective AJ upon midbody formation. Notably, in one or both tissues, Cysts (Figure 1H), Ziz (Figure 1H; Video S1I), RhoGAP1A (Figure 1H; Video S1F), Graf (Figure S3K; Video S1D), CdGAPr (Figure S3K; Video S1B), and Exn (Figure S3K; Video S1C) can be found at the rim of the cytokinetic ring, where MyoII accumulates[36] (Figure 1A). Furthermore, we found specific RhoGEF/GAPs accumulating transiently near or at the daughter cell interface during cytokinesis and *de novo* junction formation. These include Mbc (Figures 1I and 1J; Videos S1E and S1L), RhoGEF4 (Figure 1I), CdGAPr (Figures 1I and S3N; Video S1B), RhoGAP5A (Figures 1I and S3N; Videos S1G and S1N), RtGEF (Figure 1I; Video S1H), and GEFMeso (Figure S3M) both in the notum and FE, CG43102 (Figure S3M) and Exn (Figure S3M; Video S1C) in the notum, as well as RhoGAP1A (Figure 1J; Video S1M), CG46491 (Figure 1J; Video S1J), Cdep (Figure S3L), RhoGAP15B (Figure S3N; Video S1O), Zir (Figure S3N), and RhoGAP54D (Figure S3N) in the FE.

Collectively, the family-wide RhoGEF/GAP localization analyses revealed a rich spatiotemporal pattern of RhoGTPase regulators in proliferative epithelial tissues. This provides a large set of candidate regulators of cell division and junction remodeling in the polarized and multicellular context of epithelial tissues. In addition, the comparative analyses of RhoGEF/GAP localizations in two epithelial tissues are relevant to pinpoint: (1) RhoGEF/GAPs harboring similar localizations, evocative of general roles in epithelial tissues (e.g., Graf, Cysts, CdGAPr, or RhoGEF4, Figures 1B and S2A and S2B; Data S1); (2) RhoGEF/GAPs exhibiting distinct distributions, advocating for tissue-specific activities associated with the different functions and dynamics of the two epithelial tissues (e.g., RhoGAP5A, RtGEF, Cdep, and CG46491, Figures 1B and S2A and S2B; Data S1). Next, to decipher the mechanisms of epithelial cytokinesis, we decided to focus on Cysts and RhoGEF4, which showed local enrichments at different phases of junction remodeling in both tissues (Figures 1B, 1H, and 1I; Data S1). Using the aforementioned CRISPR-Cas9 plasmid library for genome editing of each RhoGEF/GAP, we generated and validated *cysts*- and *rhogef4*-null alleles to investigate their functions, mainly focusing on the notum epithelium.

The RhoGEF Cysts plays a role in mechanosensing and daughter cell membrane juxtaposition during cytokinesis

Cytokinetic ring contraction triggers a mechanosensing response in the neighboring cells associated with junctional remodeling during cytokinesis.[35,42] As defined in the notum epithelium, ring contraction induces self-organized Rok and MyoII flows and accumulations at the rim of the cytokinetic ring in the neighboring cells, thereby promoting the juxtaposition of daughter cell membranes.[36,42] During ring contraction, the Rho1 GTPase is also necessary to enhance MyoII accumulation in the neighboring cells.[42] Having uncovered that Cysts, a known guanine exchange factor (GEF) for the Rho1 GTPase in *Drosophila*,[24] is localized at the rim of the cytokinetic ring (Figures 2A and S4A; Video S2A), we decided to investigate its function in mechanosensing during cytokinesis. Interestingly, the vertebrate Cysts ortholog, p114RhoGEF, has recently been proposed to mediate mechanosensing in cultured cells,[58,59] but whether Cysts or p114RhoGEF function in mechanical responses *in vivo* or during cell division is unknown.

We first analyzed whether Cysts accumulation at the rim of the cytokinetic ring occurred in the neighboring cells. By analyzing dividing cells devoid of Cysts:GFP and neighboring Cysts:GFP-expressing cells, we observed that Cysts:GFP accumulates near the neighbor ingressing cell membrane during the cytokinesis of an adjacent dividing cell (Figure 2B; Video S2B). In addition, and as observed for MyoII[42] (Figure 2C), high-temporal-resolution time-lapse imaging revealed that Cysts:GFP speckles flowed within the ingressing membrane during furrowing (Figure 2C; Video S2C). Based on these findings, we concluded that Cysts accumulated in cells neighboring a cell undergoing cytokinesis. We then investigated whether Cysts activates the Rho1 GTPase in the neighbors during cytokinesis. We found that the Rho activity reporter (Ani-RBD:GFP[60]) is enriched in the neighboring cells within the ingressing membrane region during cytokinesis and that this enrichment required Cysts activity in the neighboring cells (Figure 2D; Video S2D).

Having found that Cysts promotes Rho1 activity in the neighboring cells at the rim of the cytokinesis ring, we then explored whether Cysts localization is a response to the force produced by the constriction of the cytokinetic ring by two different approaches. First, we acutely decreased cytokinesis force by laser ablation of the contractile ring at or after mid constriction and found that such ablation decreased Cyst:GFP accumulation in the neighbors (Figure S4B), as previously shown for MyoII acummulation.[42] Second, we observed that Cysts accumulation was decreased in cells neighboring *pnut*^{RNAi} dividing cells, which have reduced cytokinetic forces[37,38,42] (Figure 3A). If Cysts contributes to the response to contractile forces, it should regulate MyoII accumulation in the neighboring cells and daughter cell membrane juxtaposition. Indeed, in *cysts* mutant neighbors, there was a decrease in MyoII:3xmKate2 accumulation (Figures 3B and 3C; Video S2E). MyoII accumulation was less affected in *cysts* and *rho1* neighboring cells than in *rok*^{RNAi} neighboring cells (Figure 3C). This concurs with our previous finding that MyoII accumulation is only partially regulated by Rho activity since it also relies on self-organized MyoII flows due to local Ecad reduction.[42] Lastly, and in agreement with the reduction in MyoII accumulation (Figures 3B and 3C), loss of Cysts perturbed the juxtaposition of the daughter cells membranes, as manifested by the increase in the angle formed by the ingressing membranes (Figures 3B and 3D; Video S2E). Together, these observations indicate that the RhoGEF Cysts participates in mechanosensing during cell division to enhance MyoII accumulation and the juxtaposition of the daughter cell membranes.

CellPress
OPEN ACCESS

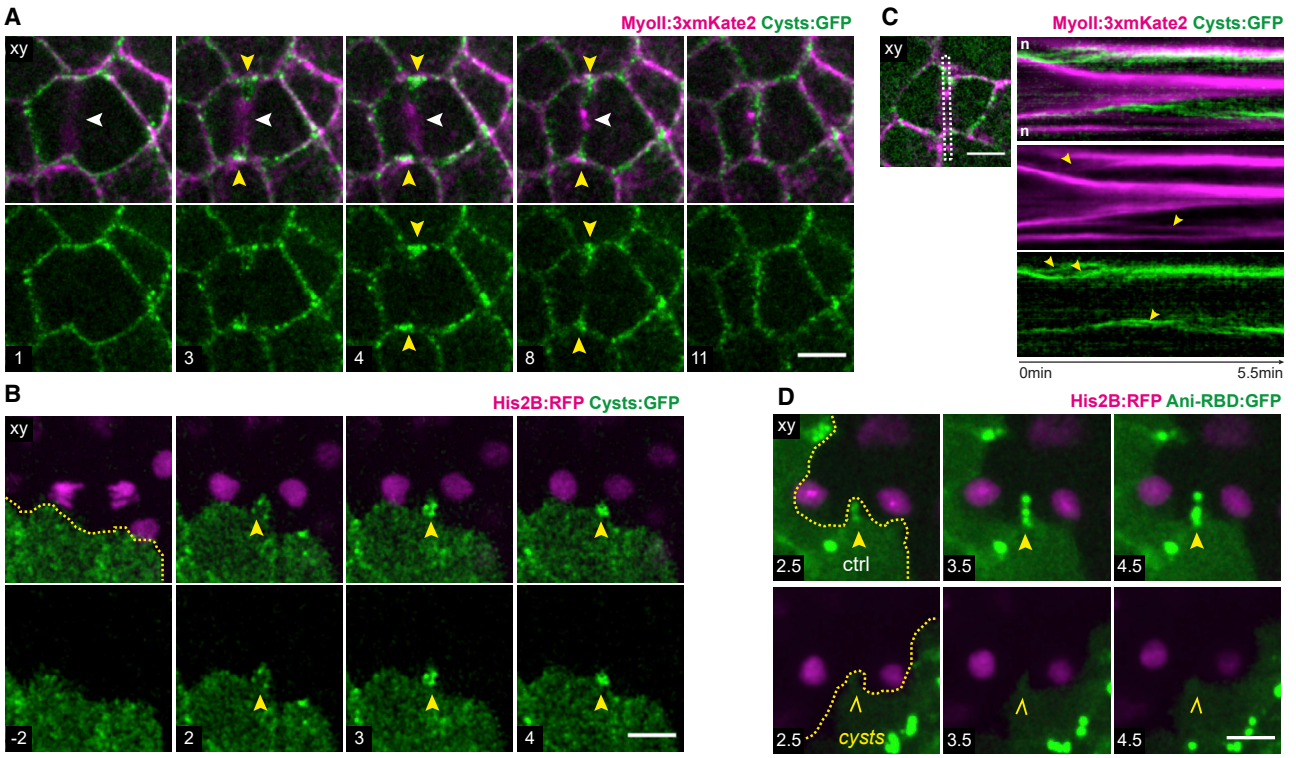

Figure 2. The RhoGEF Cysts accumulates in the neighboring cells where it activates Rho1

All images are apical top views at the level of the AJ in the notum. Unless otherwise specified, time (min, indicated in the lower left image corner) is set to 0 at the onset of cytokinesis marked by the initial deformation of AJ by the constriction of the cytokinetic ring.

(A) Time-lapse images of Cysts:GFP (top and bottom) and MyoII:3xmKate2 (top) in the dividing cell and its neighbors. White arrowheads, cytokinetic ring; yellow arrowheads, Cysts:GFP and MyoII:3xmKate2 accumulations at the rim of the cytokinetic ring.

(B) Time-lapse images of clonally expressed His2B:RFP in the dividing cell (top) and Cysts:GFP (top and bottom) in its neighbors. Images are projections of the apical surface for the GFP channel to highlight Cysts apical localization in the neighbor, merged with a projection from the apical cell surface to the nucleus for the RFP channel to visualize the dividing cell nuclei. Yellow arrowheads, Cysts:GFP accumulation within the ingressing membranes; yellow dashed line, boundary between cells expressing Cysts:GFP or His2B:RFP.

(C) Apical view of Cysts:GFP and MyoII:3xmKate2 during epithelial cell division (left) and kymograph (right) of Cysts:GFP and MyoII:3xmKate2 within the region outlined in the apical view. The kymograph shows the two sides of the ingressing membrane with outward Cysts flow toward the base of the ingressing membrane. Time (min) is set to 0 at the start of the movie. Yellow arrowheads, MyoII:3xmKate2 and Cysts:GFP speckles that flow between the ingressing membranes. As Cyst:GFP speckles flow within the ingressing membrane, they can split and fuse; see also Video S2C. n, neighboring cells.

(D) Time-lapse images of Ani-RBD:GFP and His2B:RFP in control (ctrl) and *cysts* cells neighboring a dividing cell. Ani-RBD:GFP and His2B:RFP are expressed clonally; *cysts* cells are marked by the loss of His2B:RFP signal in the bottom panels. A yellow dashed line marks the boundary between Ani-RBD:GFP-expressing and non-expressing cells. Ani-RBD:GFP was analyzed in cells adjacent to a cell that divides roughly parallel to them and devoid of Ani-RBD:GFP signal. Ani-RBD:GFP accumulation was observed in 18 out of 22 ctrl neighboring cells (81%) and in 5 out of 25 (20%) *cysts* neighboring cells. Yellow arrowheads, Ani-RBD:GFP at the rim of the cytokinetic ring in ctrl neighboring cell; yellow open arrowheads, absence of Ani-RBD:GFP accumulation in a *cysts* neighboring cell. Scale bar, 5 μm for (A)–(D).

See also Figure S4 and Video S2.

In adherent cells in culture, the Cysts vertebrate homolog p114RhoGEF is recruited to sites of Ecad accumulation upon chemical activation of MyoII or upon ectopic and global stretching of the epithelial monolayer.[58] Yet, Ecad is locally decreased in response to endogenous cytokinetic mechanical forces in *Drosophila*,[42] suggesting the existence of an additional mode of Cysts-dependent mechanosensing. To test whether endogenous cytokinetic force promotes Cysts accumulation by a local decrease of Ecad, we took advantage of two complementary approaches in interphasic cells to mirror the interphasic status of the neighboring cells. First, reduction of Ecad levels using $Ecad^{RNAi}$-mediated knockdown led to an enrichment of Cysts:GFP at cell membranes (Figure 3E). Interestingly, high-temporal-resolution time-lapse imaging showed that Ecad decrease resulted in the formation of both Cysts and MyoII flows toward the ectopic medial MyoII accumulation caused by $Ecad^{RNAi}$-mediated knockdown (Figures S4C and S4D). Second, we used the light-activated reversible inhibition by assembled trap (LARIAT) system, an optogenetic approach to promote the clustering of GFP-tagged proteins,[61,62] to generate local depletions of Ecad with high temporal control. By promoting light-induced clustering of Ecad:GFP in a tissue where Ecad:GFP was the only source of Ecad, we generated local junctional Ecad:GFP depletions and found that Cysts:mKate2 became enriched at Ecad:GFP depletion sites (Figures 3F and 3G). Together, these results indicate that Ecad decrease can promote Cysts

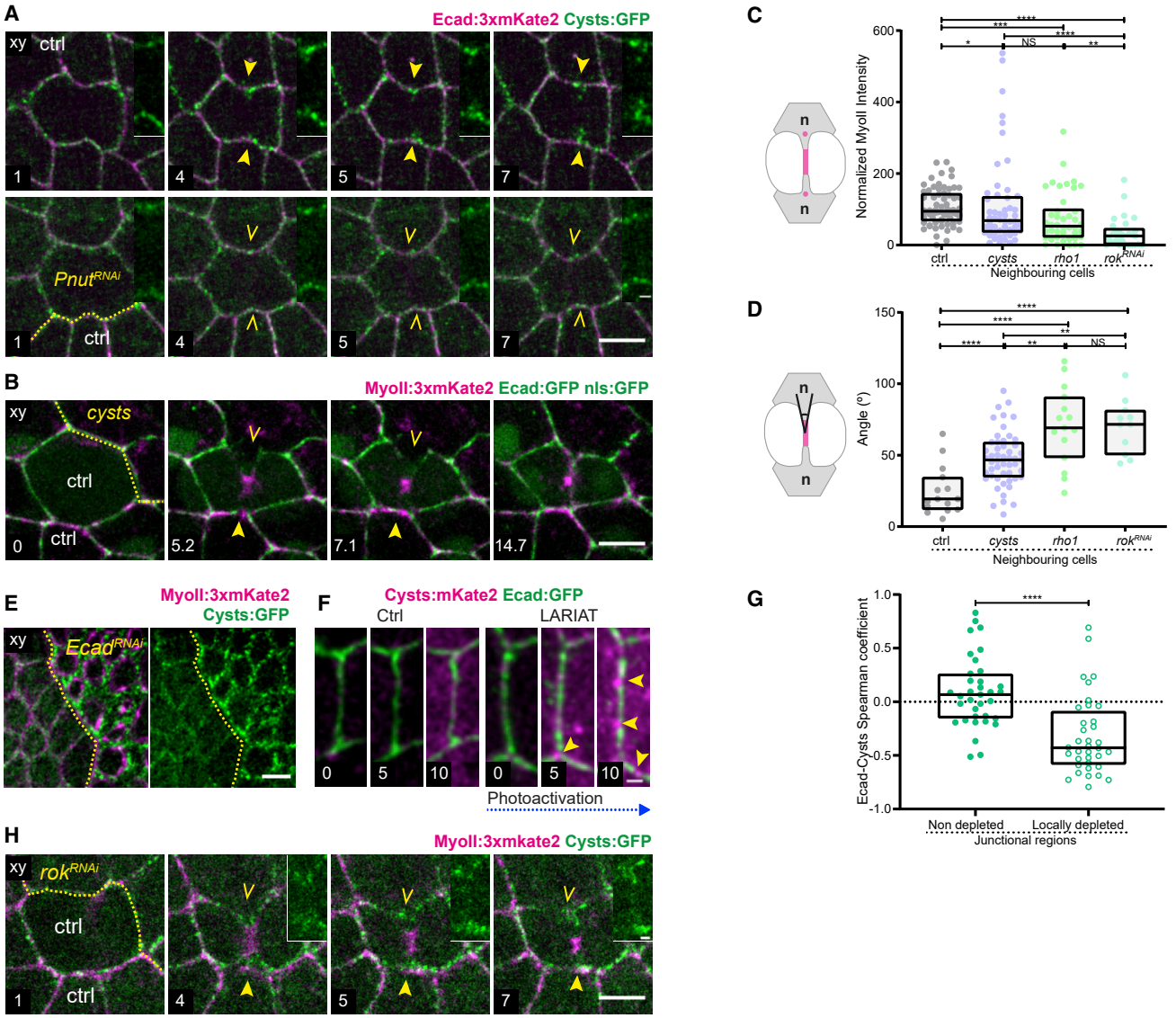

Figure 3. The RhoGEF Cysts modulates the mechanosensing response in neighboring cells and the juxtaposition of the membrane of daughter cells

All images are apical top views at the level of the AJ in the notum. Unless otherwise specified, time (min, indicated in the lower left image corner) is set to 0 at the onset of cytokinesis marked by the initial deformation of AJ by the constriction of the cytokinetic ring.

(A) Time-lapse images of Ecad:3xmKate2 and Cysts:GFP in the context of ctrl (top) and *pnut*^{RNAi} (bottom) dividing cell. *pnut*^{RNAi} cells are marked by the expression of CAAX:tBFP (not shown), and a yellow dashed line marks the boundary between ctrl and *pnut*^{RNAi} cells. Yellow arrowheads, Cysts:GFP at the rim of the cytokinetic ring in neighbors of a ctrl dividing cell; yellow open arrowheads, reduced Cysts:GFP accumulation in cells neighboring a *pnut*^{RNAi} dividing cell; insets, close-ups on Cysts:GFP signal at the rim of the cytokinetic ring in ctrl and *pnut*^{RNAi} cells. Cysts:GFP accumulation at the rim of cytokinetic ring during early cytokinesis was observed in 82% of cells neighboring a ctrl dividing cell (n = 29) and in 36% of cells neighboring *pnut*^{RNAi} dividing cells (n = 22).

(B) Time-lapse images of Ecad:GFP and MyoII:3xmKate2 in the context of a dividing cell surrounded by ctrl and *cysts* neighboring cells. *cysts* cells are marked by the loss of nls:GFP signal, and a yellow dashed line marks the boundary between ctrl and *cysts* cells. Note that nls:GFP is not visible in all ctrl cells since their nuclei can be located more basally. Yellow arrowheads, MyoII:3xmKate2 accumulation and daughter-daughter interface juxtaposition in the ctrl neighboring cell; yellow open arrowheads, reduced MyoII:3xmKate2 accumulation and delayed daughter-daughter interface juxtaposition in *cysts* neighboring cell context.

(C) Schematic of MyoII neighbor accumulation (left) and box plot of MyoII accumulation (median ± interquartile range, right) at the rim of the contractile ring at 80% of apical ring contraction in ctrl, *cysts*, *rho1*, *and rok*^{RNAi} cells neighboring a dividing cell. Note that for the *cysts* quantification, both the dividing and the neighboring cells can be *cysts* mutant cells.

(D) Schematics of the daughter-daughter interface angle (left) and box plot of the daughter-daughter interface angle (median ± interquartile range, right) at 80% of apical ring contraction in ctrl, *cysts*, *rho1*, *or rok*^{RNAi} cells neighboring a dividing cell. Note that for the *cysts* quantification, both the dividing and the neighboring cells can be *cysts* mutant cells.

(E) Images of Cysts:GFP (left and right) and MyoII:3xmKate2 (left) in a mosaic tissue with ctrl and *Ecad*^{RNAi} interphasic cells. *Ecad*^{RNAi} cells are marked by the expression of CAAX:tBFP (not shown), and the yellow dashed line marks the boundary between ctrl and *Ecad*^{RNAi} cells.

(legend continued on next page)

accumulation. Knowing that MyoII flows and accumulation depend on Rok function[36,42] and having observed that Cysts flows with MyoII within the ingressing membranes (Figure 2C), we also hypothesized that Cysts local accumulation could be reinforced by Rok. We therefore analyzed Cysts:GFP accumulation in *rok*^{RNAi} neighboring cells, which are characterized by the lack of MyoII flows and accumulation.[36,42] In the absence of Rok function, Cysts accumulation was reduced in the neighboring cells (Figure 3H). We therefore propose that Ecad dilution in response to cytokinesis forces promotes Cysts recruitment, which is reinforced by Rok activity.

In summary, we propose that the RhoGEF Cysts accumulates at the rim of the cytokinetic ring in response to a local decrease of Ecad promoted by mechanical force. In turn, Cysts is necessary to activate Rho1 and to enhance both MyoII accumulation and membranes juxtaposition prior to *de novo* junction formation, thus establishing a role for Cysts in the response to endogenous mechanical forces during epithelial cell division.

RhoGEF4 controls *de novo* AJ length upon cell division

Upon midbody formation, daughter cell membrane juxtaposition is followed by the *de novo* formation of an AJ between the two daughter cells, a feature conserved in multiple epithelial tissues including the notum and the FE.[31,32] The length and the topology of *de novo* junctions are regulated in the dividing cell by Rac, which promotes Arp2/3-dependent F-actin polymerization around the midbody and at the daughter cell interface.[36,39] In particular, F-actin polymerization propels the withdrawal of the neighboring cell membranes inserted between the daughter cells, thus enabling the formation of daughter cell junctions.[36] Yet, the mechanisms of Rac activation during epithelial cytokinesis are unknown.

To investigate how *de novo* junctions are formed upon division, we decided to focus on RhoGEF4 since it became enriched at the daughter cell interface and midbody (Figures 4A and S5C; Video S3A), mirroring the accumulation of F-actin observed in both the notum and the FE.[36,39] The human FGD3/FGD4 orthologs of RhoGEF4 remain poorly characterized despite their putative implications in cancer or Charcot-Marie Tooth disease.[63,64] Using the *rhogef4*-null allele generated by CRISPR-Cas9-mediated homologous recombination, we found that the initial junctions formed between *rhogef4* daughter cells were shorter in both tissues (Figures 4B, 4C, S5D, and S5E; Video S3B). In agreement with a role of RhoGEF4 in the dividing cells, we observed that (1) RhoGEF4 accumulation in the ring, the midbody, and the daughter cell interface is contributed by the dividing and not by the neighboring cells (Figures S5F and S5G) and (2) a short junction is formed if a *rhogef4* dividing cell is surrounded by two control cells adjacent to its cytokinetic ring (Figure S5H). These data prompted us to explore the role of RhoGEF4 in the dividing cell during cytokinesis in more detail and to investigate which RhoGTPase it regulates to control the length of junctions formed *de novo* upon division.

As RhoGEF4 localizes to different structures in the dividing cell (Figures 4A and S5A–S5C and Video S3A), we first tested whether RhoGEF4 specifically acts at the newly forming junction. During cytokinesis, RhoGEF4 localizes at the cytokinetic ring. However, we found that the loss of RhoGEF4 function did not affect the juxtaposing of the daughter cell membranes during cytokinetic ring contraction or the ring contraction rate (Figures S5I and S5J). Since RhoGEF4 also localized at the reorganizing nuclear envelope during cytokinesis, we then tested whether RhoGEF4 contributes to nuclear envelope dynamics. The dynamics of both nls:GFP and Lamin:TagRFP relocalizations to the nucleus were similar in control and *rhogef4* telophase cells (Figures S5K and S5L). Together, these data indicate that RhoGEF4 does not regulate daughter membrane juxtaposition, ring contraction, and nuclear envelope reformation, prompting us to explore how it specifically contributes to *de novo* AJ length regulation during late cytokinesis.

Toward this goal, we first analyzed Ecad dynamics during *de novo* junction formation. We found that the loss of RhoGEF4 function often caused a delay in the initial Ecad enrichment at the presumptive daughter cell interface in the notum (Figures 4B and S6A). Yet, and as previously found for the loss of function of Arp3 in the notum,[36] the occurrence of this delay did not correlate with a reduced junction length (Figure S6A). In addition, the timing of Ecad accumulation was unaffected in *rhogef4* cells in the FE (Figure S6B). Together, these findings indicate that RhoGEF4 regulates AJ length independently of the accumulation dynamics of Ecad at the daughter cell interface. We therefore hypothesized that RhoGEF4 regulates AJ length by controlling the withdrawal of neighboring cell membranes before junction formation. The dynamics of the daughter and neighbor cell membranes can be tracked by differently labeling the dividing and neighbor cell membranes with PH:GFP and PH:chFP. Using this approach, we first found that control and *rhogef4* cells neighboring control dividing cells withdrew their membrane with the same dynamics (Figures S6C and S6D), confirming that RhoGEF4 is dispensable in the neighboring cells. Second, we observed that the membrane withdrawal of control cells neighboring *rhogef4* dividing cells was significantly delayed (Figures 4D and 4E). Altogether, we propose that RhoGEF4 is

(F) Time-lapse images of Ecad:GFP and Cysts:mKate2 in the absence (left) and the presence of LARIAT (right). Time is set to 0 at the beginning of imaging or photoactivation. Yellow arrowheads, Cysts:mKate2 accumulation within Ecad:GFP depletion regions. The brightness contrast for the Cysts:mKate2 signal was differentially set between ctrl and LARIAT. The increase in Cysts:mKate2 signal in both conditions is due to the use of the bleach correction function in Fiji on the low Cysts:mKate2 signal.

(G) Box plot of the Spearman correlation coefficients between Ecad:GFP and Cysts:mKate2 signals in junctional regions without local Ecad:GFP depletion (full circles) or in junctional regions encompassing an Ecad depletion (open circles) upon LARIAT optogenetic activation.

(H) Time-lapse images of MyoII:3xmKate2 and Cysts:GFP in the context of a ctrl dividing cell surrounded by ctrl and *rok*^{RNAi} neighboring cells. *rok*^{RNAi} cells are marked by the expression of CAAX:tBFP (not shown), and the yellow dashed line marks the boundary between ctrl and *rok*^{RNAi} cells. Yellow arrowheads, Cysts:GFP accumulation in the ctrl neighboring cells; yellow open arrowheads, reduced Cysts:GFP accumulation in the *rok*^{RNAi} neighbors; inset, close-ups on Cysts:GFP signal at the rim of the cytokinetic ring. Ratios of Cysts:GFP levels between the *rok*^{RNAi} and ctrl neighbors have a median value of 0.44 and an interquartile range from 0.2 to 0.7 (n = 26).

Scale bar, 5 μm for (A), (B), (E) and (H) 1 μm for (F) and insets in (A) and (H). Mann-Whitney tests: *p < 0.05; **p < 0.01; ***p < 0.001; ****p < 0.0001.

See also Figure S4 and Video S2. For details on quantifications, see STAR Methods.

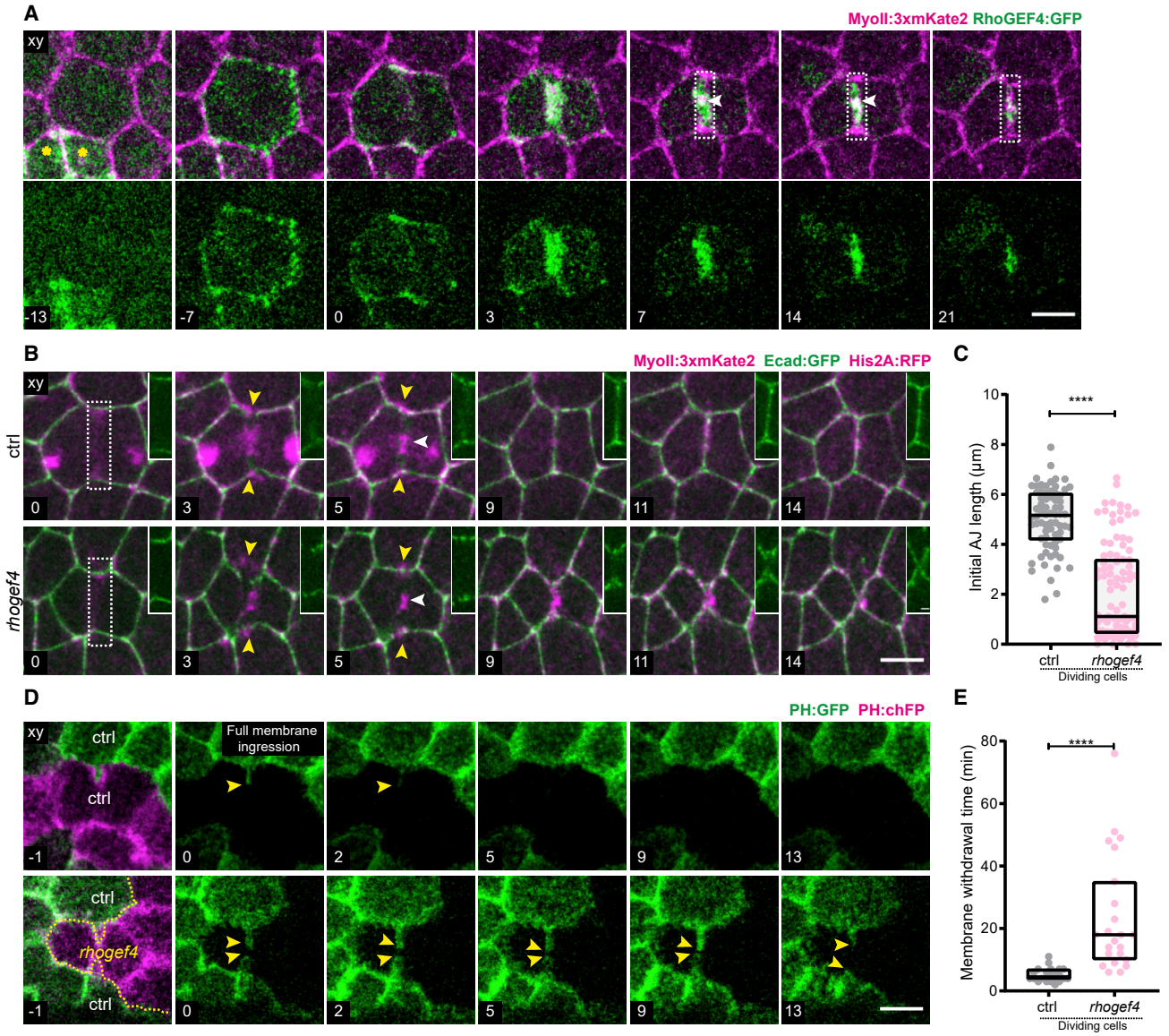

Figure 4. RhoGEF4 regulates *de novo* cell junction length upon cytokinesis

All confocal images are apical top views at the level of the AJ in the notum. Unless otherwise specified, time (min, indicated in the lower left image corner) is set to 0 at the onset of cytokinesis marked by the initial deformation of AJ by the constriction of the cytokinetic ring.

(A) Time-lapse images of RhoGEF4:GFP (top and bottom) and MyoII:3xmKate2 (top) from interphase to late cytokinesis. White arrowheads, midbody; white dashed box, daughter cell interface. The yellow asterisks indicate two neighboring cells in late cytokinesis.

(B) Time-lapse images of Ecad:GFP, MyoII:3xmKate2, and His2A:RFP in ctrl and *rhogef4* dividing cells. Inset, close-up on the Ecad:GFP signal along the daughter cell interface formed during cytokinesis in the region marked by the white dashed box. White arrowheads, midbody; yellow arrowheads, MyoII accumulation in the neighboring cells and prospective position of *de novo* daughter-daughter cell junction. Ctrl and *rhogef4* cells are marked by the presence and absence of His2A:RFP signal, respectively. Since the nuclei can be located basal to the confocal section shown, the His2A:RFP signal is not visible in all panels or ctrl cells.

(C) Box plot of *de novo* AJ length (median ± interquartile range) in ctrl and *rhogef4* cells.

(D) Time-lapse images of clonally expressed PH:GFP and PH:chFP in a ctrl dividing cell (marked by PH:chFP) surrounded by ctrl cells (top) and in a *rhogef4* dividing cell (marked by PH:chFP) surrounded by ctrl neighboring cells (bottom). Time (min) is set to 0 at the time of full neighboring membrane ingression. The dividing cell membranes are only shown in the first panel. *rhogef4* cells are marked by the absence of PH:GFP expression, and the yellow dashed line outlines the boundary between *rhogef4* and ctrl cells. Yellow arrowheads, position of the tip of the neighboring membranes inserted between the two daughter cells.

(E) Box plot of the duration of ctrl neighboring cell membrane withdrawal (median ± interquartile range) from the dividing ctrl or *rhogef4* daughter cell apical interfaces.

Scale bar, 5 µm for (A), (B), and (D) and 1 µm for inset in (B). Mann-Whitney test: ****$p < 0.0001$.

See also Figures S5 and S6 and Video S3. For details on quantifications, see STAR Methods.

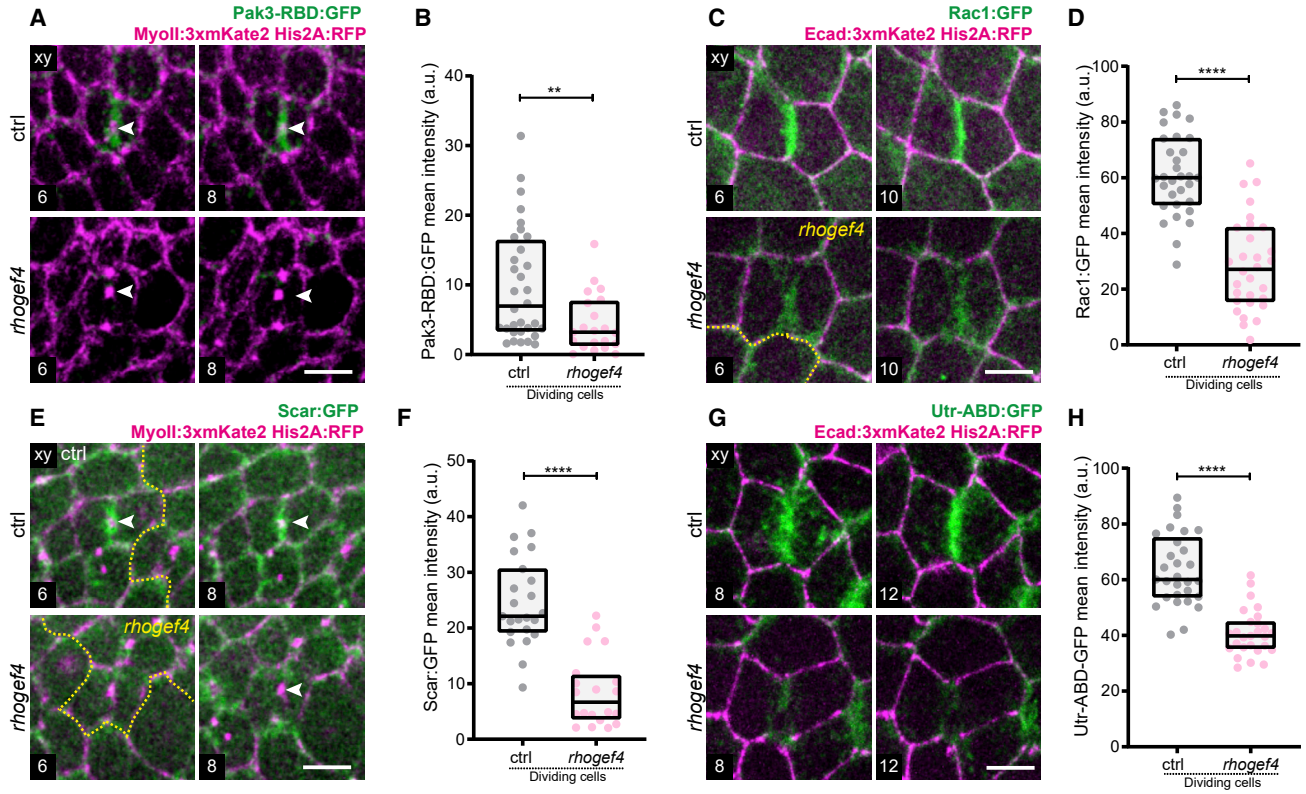

Figure 5. RhoGEF4 regulates Rac and F-actin at the daughter cell interface in late cytokinesis

All confocal images are apical top views at the level of the AJ in the notum. Unless otherwise specified, time (min, indicated in the lower left image corner) is set to 0 at the onset of cytokinesis marked by the initial deformation of AJ by the constriction of the cytokinetic ring. In (A), (C), (E), and (G), ctrl and *rhogef4* cells are marked by the presence and absence of His2A:RFP signal, respectively. Since the nuclei can be located basal to the confocal section shown, the His2A:RFP signal is not visible in all panels of ctrl cells.

(A) Time-lapse images of MyoII:3xmKate2 and Pak3-RBD:GFP for ctrl and *rhogef4* dividing cells during cytokinesis. White arrowheads, midbody.

(B) Box plot of Pak3-RBD:GFP intensity (median ± interquartile range) at the apical daughter cell interface in ctrl and *rhogef4* cells.

(C) Time-lapse images of Ecad:3xmKate2 and Rac1:GFP in ctrl and *rhogef4* dividing cells during cytokinesis. The yellow dashed line outlines the boundary between *rhogef4* and ctrl cells.

(D) Box plot of Rac1:GFP intensity (median ± interquartile range) at the apical daughter cell interface in ctrl or *rhogef4* daughter cells during late cytokinesis.

(E) Time-lapse images of Scar:GFP and MyoII:3xmKate2 in ctrl and *rhogef4* dividing cells during cytokinesis. White arrowheads, midbody. The yellow dashed line outlines the boundary between *rhogef4* and ctrl cells.

(F) Box plot of Scar:GFP intensity (median ± interquartile range) at the apical daughter cell interface in ctrl or *rhogef4* daughter cells.

(G) Time-lapse images of Ecad:3xmKate2 and Utr-ABD:GFP in ctrl and *rhogef4* dividing cells during cytokinesis.

(H) Box plot of Utr-ABD:GFP intensity (median ± interquartile range) at the apical daughter cell interface in ctrl or *rhogef4* daughter cells.

Scale bar, 5 μm for (A), (C), (E) and (G). Mann-Whitney test: ****$p < 0.0001$. **$p < 0.01$.

See also Figure S6 and Video S3. For details on quantifications, see STAR Methods.

necessary in the dividing cells to promote the withdrawal of the neighboring membranes, thereby controlling *de novo* AJ length.

RhoGEF4 can act as a GEF for Rac or Rho *in vitro*.[65] We therefore tested whether RhoGEF4 regulates Rac or Rho1 activities in the control of neighboring membrane withdrawal. Toward this end, we compared the dynamics of the Rho activity reporter Ani-RBD:GFP and of a Rac activity reporter (Pak3-RBD:GFP[66]) during cytokinesis. In control dividing cells, Ani-RBD:GFP was strongly enriched at the contractile ring and the midbody (Figure S6E), whereas Pak3-RBD:GFP was present at the daughter cell interface before *de novo* junction formation (Figure 5A). While Ani-RBD:GFP localization was unaffected in *rhogef4* cells (Figures S6E and S6F), the Pak3-RBD:GFP signal was reduced at the daughter cell interface in *rhogef4* cells (Figures 5A and 5B). Further confirming the role of RhoGEF4 in controlling Rac function, we found that (1) the loss of RhoGEF4 function led to a decrease of Rac1:GFP at the daughter cell interface (Figures 5C and 5D; Video S3C) and (2) Scar, a downstream effector of Rac and an Arp2/3 activator,[67] was also decreased at the daughter cell interface of *rhogef4* cells (Figures 5E and 5F). Finally, as observed upon reduction of Rac function,[36] the utrophin-ABD:GFP F-actin probe was strongly reduced at the daughter cell interface in *rhogef4* dividing cells (Figures 5G and 5H; Video S3D). Together, these data indicate that RhoGEF4 acts in the dividing cell to regulate *de novo* AJ length by controlling F-actin accumulation via Rac at the daughter cell interface to induce neighboring cell membrane withdrawal.

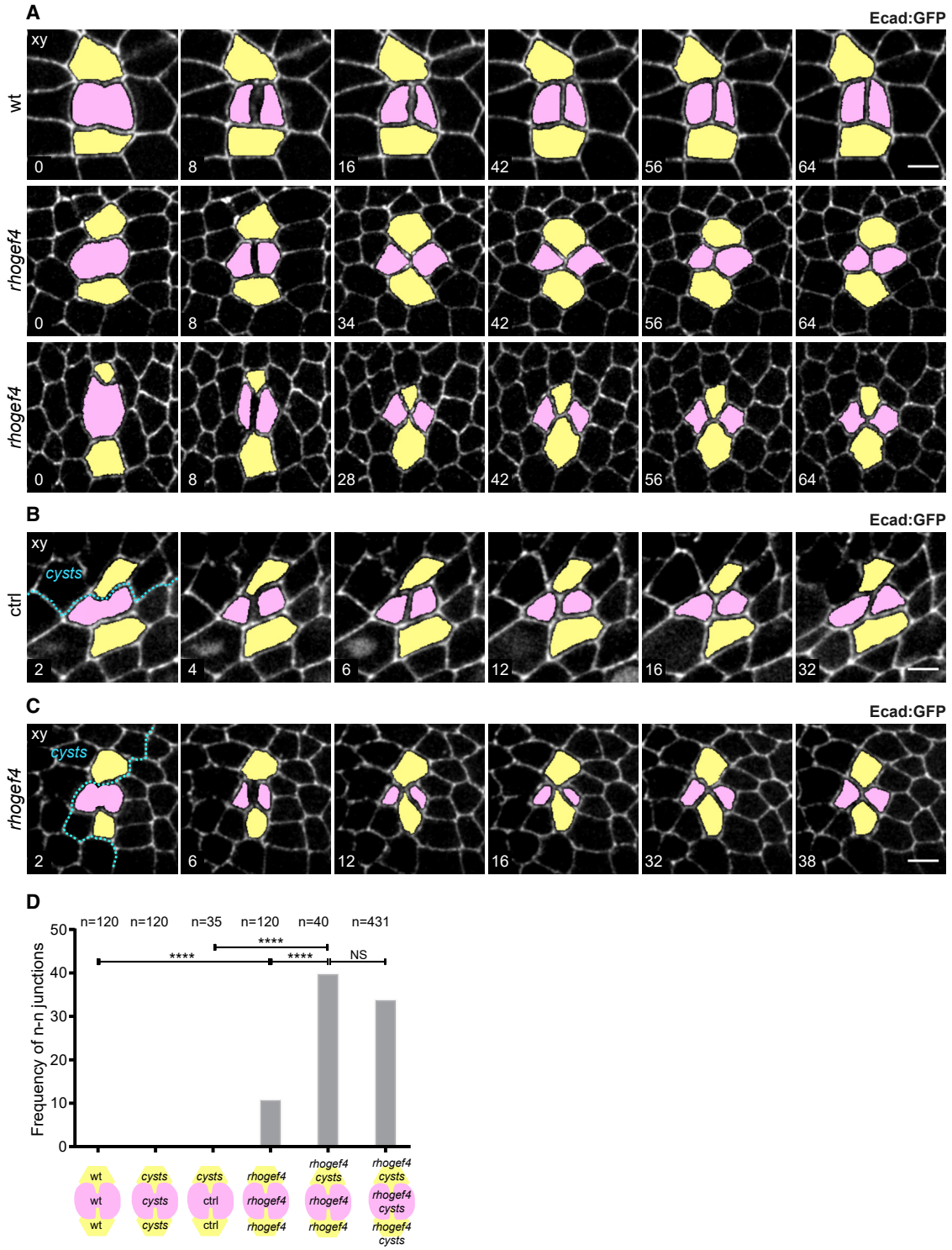

Figure 6. RhoGEF4 and Cysts synergistically control junction topology upon cell division

All images are apical top views of the notum epithelium at the level of the AJ labeled by Ecad:GFP. The dividing and daughter cells are colored in pink, while the neighboring cells are in yellow. Unless otherwise indicated, time (min, indicated in the lower left image corner) is set to 0 at the onset of cytokinesis marked by the initial deformation of AJ by the constriction of the cytokinetic ring. In (B) and (C), ctrl and *cysts* cells are marked by the presence and absence of nls:GFP signal, respectively. Since the nuclei can be located basal to the confocal section shown, the nls:GFP signal is not visible in all panels or ctrl cells.

(A) Time-lapse images of Ecad:GFP from cytokinesis onward in wt (top) or *rhogef4* (middle and bottom) pupae. Two examples are shown for *rhogef4* tissues: in the middle panels, a d-d junction is formed upon cell division (from t = 34 min onward), whereas in the bottom ones, a n-n junction is formed (from t = 30 min onward).

(legend continued on next page)

RhoGEF4 and Cysts cooperate in defining the initial *de novo* junction topology

Upon cytokinesis, two distinct topological AJ arrangements have been reported in different epithelia: a daughter-daughter (d-d) AJ or neighbor-neighbor (n-n) AJ.[31–35,37,39,41,68,69] Having found that RhoGEF4 is a key regulator of the length of the AJ between daughter cells, we analyzed whether the loss of RhoGEF4 modulates the topology of cell arrangements upon cytokinesis. Although a d-d AJ is always directly formed upon cell division in wild-type (wt) cells (n = 120), we found that in a fraction of *rhogef4* cells in the notum (11%, n = 120), an AJ is transiently formed between the neighboring cells instead of the two daughter cells (Figures 6A and 6D; Video S3E). Importantly, the formation of an n-n AJ did not correlate with the timing of Ecad enrichment at the initial interface (Figure S6G) and was rather associated with the formation of an initial very short d-d contact (i.e., less than 1 μm). We also found that the impact of RhoGEF4 loss of function on the length of the d-d junction was stronger in the notum than in the FE, where the very short d-d junctions that could promote topological defects were unfrequently observed (2 cases out of 19 divisions). While this could be due to compensatory mechanisms associated with the function of other RhoGEF localized at the d-d interface in the FE, we recalled that in contrast to the FE, the notum undergoes major morphological changes during proliferation.[43,46,47] We thus hypothesized that in tissues undergoing major morphogenesis movements, the loss of RhoGEF4 function could lead to the formation of very short junctions and thus transient n-n junctions. We therefore analyzed the impact of RhoGEF4 loss of function in the pupal histoblast and wing, two epithelial tissues characterized by proliferation and large morphogenetic movements.[46,68,70–73] Strikingly, in both tissues, the loss of RhoGEF4 function led to very short AJ formation and topological defects during cell division (Figures S6H–S6J). So far, the topology of AJ formed upon cell division has been proposed to regulate tissue dynamics and planar cell polarity[33,41,68]; our results support the notion that the overall dynamics of epithelial tissues can also contribute to the initial topology of the junctions formed upon cytokinesis.

Having identified two RhoGEFs regulating membrane juxtaposition during ring contraction and membrane withdrawal upon midbody formation, respectively, we could then investigate, for the first time, whether these two processes cooperate to regulate the topology of the newly formed AJ. Toward this goal, we analyzed whether, in *rhogef4* tissues, the proportion of topological defects upon cytokinesis increases when *rhogef4* dividing cells are neighbored by a cell also mutant for *cysts*. Under these conditions, the proportion of the n-n AJ increased by 3.6-fold relative to *rhogef4* dividing cells neighboring cells devoid of *cysts* mutation (Figures 6C and 6D). Since control dividing cells neighbored by a *cysts* cell never formed n-n AJ (0%, n = 35, Figures 6B and 6D), our results revealed a synergistic role of RhoGEF4 and Cysts in the control of AJ topology during cytokinesis. Together, we conclude that daughter cell membrane juxtaposition facilitated by Cysts via Rho and neighboring membrane withdrawal mediated by RhoGEF4 via Rac coregulate *de novo* junction formation and topology during epithelial cell division *in vivo*.

DISCUSSION

By modulating the activity of small RhoGTPases, RhoGEFs and RhoGAPs control cytoskeleton organization and dynamics in a broad range of processes such as cell morphogenesis, division, and migration in all eukaryotes.[4–7,11,12] The functions of RhoGTPases have been extensively and systematically investigated in individual cells. However, multicellularity entails a complex interplay between the cytoskeleton and cell-cell junctions to regulate cell and tissue architecture and dynamics,[7,74] thus highlighting the relevance of characterizing RhoGEF/GAP function in tissues. Cell division has emerged as a multicellular process since it entails the deformation of the neighboring cells, the remodeling of the dividing and neighbor cell junctions, and *de novo* junction formation.[31,32] To better understand how RhoGEFs and RhoGAPs control the cytoskeleton and cell junction dynamics in proliferative epithelial tissues, we have generated a family-wide *Drosophila* transgenic library of fluorescently tagged RhoGEF/GAPs and systematically determined their distributions during interphase and cell division in two epithelial tissues. Our screen revealed multiple uncharacterized RhoGEF/GAP interphasic localizations as well as a complex choreography of RhoGEF/GAPs during cell division. Building on our screen, we have better defined the processes of mechanosensing and junction formation by delineating how the activities of specific RhoGTPases are controlled during epithelial cytokinesis and *de novo* junction formation. We have therefore uncovered the first mechanisms of RhoGTPase activation underlying the multicellularity of epithelial cell division.

It is now well established that cytokinesis and, more generally, cell division entail a mechanosensing response in the neighbors.[35,42,75] Despite such conserved mechanical responses and the proposed roles of RhoGTPases in mechanosensing,[76] the nature of the RhoGEF associated with the response to cytokinesis ring contraction has remained unknown. Our work establishes that the RhoGEF Cysts modulates the response to endogenous mechanical forces generated by ring contraction in the neighboring cells, thereby enhancing daughter cell membrane juxtaposition. We previously reported that ring contractile forces are sensed by the local decrease of Ecad.[42] Since we found that reducing the level of Ecad is sufficient to promote Cysts accumulation, Cysts response to mechanical force can be directly caused by the decrease in Ecad during ring contraction. In addition, MyoII

(B) Time-lapse images of Ecad:GFP from cytokinesis onward of a control (ctrl) dividing cell neighboring *cysts* and ctrl cells. *cysts* cells are marked by the absence of nls:GFP signal, and the cyan dashed line outlines the boundary between *cysts* and ctrl cells.
(C) Time-lapse images of Ecad:GFP from cytokinesis onward of a *rhogef4* dividing cell neighboring *rhogef4,cysts* or *rhogef4* cells. *cysts* cells are marked by the absence of nls:GFP signal, and the cyan dashed line outlines the boundary between *cysts,rhogef4* and *rhogef4* cells.
(D) Graph of the frequency of n-n junctions formed upon cell division in wt, *cysts*, ctrl, *rhogef4*, or double *cysts*,*rhogef4* mutant dividing cells neighboring wt, *cysts*, ctrl, *rhogef4*, or double *rhogef4*,*cysts* mutant cells, respectively, as indicated in the schematics below the graph.
Scale bar, 5 μm for (A), (B), and (D) and 1 μm for inset in (B). Mann-Whitney test: ****$p \leq 0.0001$.
See also Figure S6 and Video S3. For details on quantifications, see STAR Methods.

flows and accumulation can also promote Rho local activation,[60,77] and Cysts recruitment at the rim of the cytokinesis ring depends on Rok. Thus, the Cysts response to mechanical force can be also indirectly caused by the Rok and MyoII accumulation due to the Ecad decrease. Interestingly, whereas previous studies in cell culture showed that the Cysts ortholog p114RhoGEF is recruited at sites of Ecad accumulation,[58] we uncovered an additional mechanism of Cysts localization promoted by local Ecad decrease due to mechanical forces. To further understand how cells respond to mechanical forces associated with a local Ecad decrease, it will be relevant to explore how Cysts is recruited to sites of lower Ecad and how Rok-dependent contractility feedbacks on Cysts dynamics. Notably, at least two distinct Ecad dynamics have been observed during epithelial cytokinesis in vertebrates.[33,35] In the avian embryo at stage EGK-X, cell division is concomitant to a local depletion of basal Ecad and an accumulation of MyoII and F-actin,[33] whereas in *Xenopus*, ring contraction triggers a well-known force-sensing response associated with the accumulation of Ecad and Vinculin.[35] Building on our findings on Cysts and the ones on p114RhoGEF *in vitro*,[58] one could hypothesize that Cysts/p114RhoGEF represents a common platform for the response to mechanical force during cytokinesis, thus calling for the investigation of the function of RhoGTPases in cells neighboring the dividing cells in vertebrates. We found that in response to cytokinesis forces, *cyst*s and *rho1* mutants showed a similar decrease in MyoII accumulation but that the *rho1* phenotype on junction juxtaposition was stronger. Cysts is therefore a major regulator of Rho1 to regulate MyoII accumulation, but our data also suggest that Rho1 plays an additional Cysts-independent function in the control of membrane juxtaposition during cytokinesis. Lastly, Cysts is involved in AJ integrity, cell-cell rearrangements, and cell ingression in interphasic cells in the early *Drosophila* embryo,[20,24,78] which are processes entailing the production of mechanical forces and the remodeling of the actomyosin cytoskeleton.[74,76,79] One could therefore envision that cytoskeleton and junction dynamics might also depend on the Cysts mechanosensing activity in these developmental processes.

De novo junction formation is inherent to the proliferation of epithelia. *In vitro* experiments have put forward a fundamental role for Rac in modulating the dynamics of junction formation upon cell-cell contact formation.[80–82] Previous findings have also underscored a role for Rac activity in cytokinesis regulating both ring constriction and the topology of the daughter-daughter cell interface.[36,83] Here, we uncovered that RhoGEF4 promotes the localization of active Rac at the daughter-daughter cell interface to ensure the withdrawal of the neighboring cell membranes. Therefore, RhoGEF4 is a regulator of Rac function in the control of *de novo* junction length, as well as of the dynamics of the cell-cell arrangements upon cytokinesis. By comparing the role of RhoGEF4 in different tissues, our work also suggests that the initial topology of the junction formed upon cytokinesis can be modulated by the overall dynamics or mechanical properties of epithelial tissues. Lastly, by combining loss of Cysts and RhoGEF4 function, we establish that the topology of *de novo* junctions formed upon cell division is synergistically regulated both by membrane juxtaposition during ring constriction and by membrane withdrawal upon midbody formation. Altogether, our analyses of Cysts and RhoGEF4 functions provide a far better understanding of the mechanisms of Rho and Rac regulation during epithelial cell division, and they illustrate how their distinct activations in the dividing and neighboring cells couple cytokinesis and junction formation.

Our findings on Cysts and RhoGEF4 also highlight the relevance of screening fluorescently tagged libraries to pinpoint key regulators of small GTPases necessary for cytoskeleton and junctional regulations *in vivo*. In particular, we foresee that family-wide characterization of RhoGEF/GAP localization and dynamics will be instrumental to better understand numerous aspects of the conserved process of cell division in invertebrates and vertebrates. So far, studies on cell division have mainly focused on the roles of two RhoGTPase regulators, ECT2 (*Drosophila* Pbl) and RACGAP1 (*Drosophila* Tum).[1,27–30,54] Our systematic analysis now uncovered a very diverse set of RhoGEF/GAP localizations during epithelial cell division. Accordingly, our screen suggested several possible avenues to decipher the function of RhoGEF/GAPs in mitotic rounding, polar relaxation, and asymmetric furrowing, as well as in midbody dynamics. We also observed that several RhoGEF/GAPs display similar localizations. These findings will be instrumental to design double or triple loss-of-function experiments to explore RhoGEF/GAP functions and to complement loss-of-function screens that would overlook specific RhoGEF/GAP functions due to their functional redundancy. In addition, our analysis in two distinct tissues underscores a set of RhoGEF/GAPs with different localization and dynamics. This illustrates the relevance of the *in vivo* exploration under the control of the endogenous promoters to explore how mitosis and cytoskeleton dynamics are differentially modulated to regulate tissue development or function. More generally, RhoGTPases are central regulators of cell and tissue dynamics in metazoans[4–6]; we therefore expect that the library will be a key resource to dissect RhoGTPase spatiotemporal regulation and function in a variety of developmental, homeostatic, and repair contexts in epithelia, as well as in stem cells, migrating cells, and neurons.

STAR★METHODS

Detailed methods are provided in the online version of this paper and include the following:

- KEY RESOURCES TABLE
- RESOURCE AVAILABILITY
  - Lead contact
  - Materials availability
  - Data and code availability
- EXPERIMENTAL MODEL AND SUBJECT DETAILS
  - Fly husbandry and stocks
- METHOD DETAILS
  - Molecular Biology and Transgenesis
  - Transgenic Fluorescently tagged RhoGEF/GAP Library
  - Plasmid Library for generating RhoGEF/GAP deletion RMCE alleles
  - Genetics, somatic clones and RNA interference
  - Pupa and egg chamber mounting for imaging
  - Microscopy
  - Localization screen of tagged RhoGEF/GAPs in epithelial tissues
  - Optogenetics

- Laser ablation of the cytokinetic ring
- QUANTIFICATION AND STATISTICAL ANALYSIS
  - Dynamics of cytokinesis, membrane juxtaposition and AJ formation
  - Fluorescent reporter signal levels
  - Figure preparation
  - Sampling and Statistics

SUPPLEMENTAL INFORMATION

Supplemental information can be found online at https://doi.org/10.1016/j.cub.2023.01.028.

ACKNOWLEDGMENTS

We thank T. Lecuit, F. Pichaud, M. Suzanne, Bloomington Stock Centre, Vienna Drosophila Resource Center, Transgenic RNAi Project at Harvard Medical School, and Kyoto Stock Center for fly lines; L. Alpar, M. Balakireva, and F. Bosveld for critical comments on the manuscript; F. Macaluso for help with experiments characterizing RhoGEF4 function; A.F. Santos and A. Barros-Carvalho for help with the production of RhoGEF lines; the PICT-IbiSA@BDD imaging facility of Institut Curie (member of the French National Research Infrastructure France-BioImaging, ANR-10-INBS-04); the i3S Scientific Platform ALM, member of the national infrastructure PPBI, Portuguese Platform of Bioimaging (PPBI-POCI-01-0145-FEDER-022122); ERC Advanced (TiMorph, 340784); ARC (SL220130607097); ANR (TiMecaDiv 20CE13000801), CANCERO-INCA (PLBIO2020/BELLAICHE); ANR Labex DEEP (11-LBX-0044, PSL ANR-10-IDEX-0001-02); Fundação para a Ciência e a Tecnologia, I.P. (PTDC/BIA-CEL/1511/2021, PTDC/BEX-BCM/0432/2014) grants for funding. F.d.P. was supported by a FRM post-doctoral fellowship (SPF20170938661); M.O. was supported by a PhD fellowship from FCT and the post-doctoral salary by the Maria de Sousa Award (48/2021).

AUTHOR CONTRIBUTIONS

Experiments, F.d.P., M.O., J.M.D.I.H., I.C., J.L.-G., and Z.W.; data analysis, F.d.P., M.O., J.M.D.I.H., I.C., and J.L.-G.; methodology, C.M., I.G., and S.P.; resources, I.G., S.P, C.M., J.M.D.I.H., M.O., F.d.P, and A.L.; visualization, F.d.P., M.O., and E.M.-d-S.; writing – original draft, F.d.P., I.C., Y.B., and E.M.-d.-S.; writing – review & editing, F.d.P., Y.B., M.O., I.C., E.M.-d.-S., S.P., and J.M.D.I.H.; supervision, Y.B. and E.M.-d.-S.; project administration, Y.B. and E.M.-d.-S.; funding acquisition, Y.B., F.d.P., and E.M.-d.-S.

DECLARATION OF INTERESTS

The authors declare no competing interests

Received: October 18, 2022
Revised: December 30, 2022
Accepted: January 16, 2023
Published: February 10, 2023

REFERENCES

1. Glotzer, M. (2017). Cytokinesis in metazoa and fungi. Cold Spring Harb. Perspect. Biol. *9*, a022343.
2. Cadart, C., Zlotek-Zlotkiewicz, E., Le Berre, M., Piel, M., and Matthews, H.K. (2014). Exploring the function of cell shape and size during mitosis. Dev. Cell *29*, 159–169.
3. Taubenberger, A.V., Baum, B., and Matthews, H.K. (2020). The mechanics of mitotic cell rounding. Front. Cell Dev. Biol. *8*, 687.
4. Arnold, T.R., Stephenson, R.E., and Miller, A.L. (2017). Rho GTPases and actomyosin: partners in regulating epithelial cell-cell junction structure and function. Exp. Cell Res. *358*, 20–30.
5. Heasman, S.J., and Ridley, A.J. (2008). Mammalian Rho GTPases: new insights into their functions from in vivo studies. Nat. Rev. Mol. Cell Biol. *9*, 690–701.
6. Jaffe, A.B., and Hall, A. (2005). Rho GTPases: biochemistry and biology. Annu. Rev. Cell Dev. Biol. *21*, 247–269.
7. Buckley, C.E., and St Johnston, D. (2022). Apical–basal polarity and the control of epithelial form and function. Nat. Rev. Mol. Cell Biol. *23*, 559–577.
8. Lechler, T., and Mapelli, M. (2021). Spindle positioning and its impact on vertebrate tissue architecture and cell fate. Nat. Rev. Mol. Cell Biol. *22*, 691–708.
9. Godard, B.G., and Heisenberg, C.P. (2019). Cell division and tissue mechanics. Curr. Opin. Cell Biol. *60*, 114–120.
10. Jülicher, F., and Eaton, S. (2017). Emergence of tissue shape changes from collective cell behaviours. Semin. Cell Dev. Biol. *67*, 103–112.
11. Iden, S., and Collard, J.G. (2008). Crosstalk between small GTPases and polarity proteins in cell polarization. Nat. Rev. Mol. Cell Biol. *9*, 846–859.
12. Denk-Lobnig, M., and Martin, A.C. (2019). Modular regulation of Rho family GTPases in development. Small GTPases *10*, 122–129.
13. Hodge, R.G., and Ridley, A.J. (2016). Regulating Rho GTPases and their regulators. Nat. Rev. Mol. Cell Biol. *17*, 496–510.
14. Lawson, C.D., and Ridley, A.J. (2018). Rho GTPase signaling complexes in cell migration and invasion. J. Cell Biol. *217*, 447–457.
15. Jordan, S.N., and Canman, J.C. (2012). Rho GTPases in animal cell cytokinesis: an occupation by the one percent. Cytoskeleton (Hoboken) *69*, 919–930.
16. Bagci, H., Sriskandarajah, N., Robert, A., Boulais, J., Elkholi, I.E., Tran, V., Lin, Z.Y., Thibault, M.-P., Dubé, N., Faubert, D., et al. (2020). Mapping the proximity interaction network of the Rho-family GTPases reveals signalling pathways and regulatory mechanisms. Nat. Cell Biol. *22*, 120–134.
17. Zihni, C., Munro, P.M.G., Elbediwy, A., Keep, N.H., Terry, S.J., Harris, J., Balda, M.S., and Matter, K. (2014). Dbl3 drives Cdc42 signaling at the apical margin to regulate junction position and apical differentiation. J. Cell Biol. *204*, 111–127.
18. Toret, C.P., Collins, C., and Nelson, W.J. (2014). An Elmo-Dock complex locally controls Rho GTPases and actin remodeling during cadherin-mediated adhesion. J. Cell Biol. *207*, 577–587.
19. Nakajima, H., and Tanoue, T. (2011). Lulu2 regulates the circumferential actomyosin tensile system in epithelial cells through p114RhoGEF. J. Cell Biol. *195*, 245–261.
20. Garcia De Las Bayonas, A., Philippe, J.M., Lellouch, A.C., and Lecuit, T. (2019). Distinct RhoGEFs activate apical and junctional contractility under control of G proteins during epithelial morphogenesis. Curr. Biol. *29*, 3370–3385.e7.
21. Mason, F.M., Xie, S., Vasquez, C.G., Tworoger, M., and Martin, A.C. (2016). RhoA GTPase inhibition organizes contraction during epithelial morphogenesis. J. Cell Biol. *214*, 603–617.
22. Fic, W., Bastock, R., Raimondi, F., Los, E., Inoue, Y., Gallop, J.L., Russell, R.B., and St Johnston, D. (2021). RhoGAP19D inhibits Cdc42 laterally to control epithelial cell shape and prevent invasion. J. Cell Biol. *220*, e202009116.
23. Laurin, M., Gomez, N.C., Levorse, J., Sendoel, A., Sribour, M., and Fuchs, E. (2019). An RNAi screen unravels the complexities of rho GTPase networks in skin morphogenesis. Elife *8*, 1–34.
24. Silver, J.T., Wirtz-Peitz, F., Simões, S., Pellikka, M., Yan, D., Binari, R., Nishimura, T., Li, Y., Harris, T.J.C., Perrimon, N., and Tepass, U. (2019). Apical polarity proteins recruit the RhoGEF Cysts to promote junctional myosin assembly. J. Cell Biol. *218*, 3397–3414.
25. Toret, C.P., Shivakumar, P.C., Lenne, P.F., and Le Bivic, A. (2018). The ELMO-MBC complex and RhoGAP19D couple rho family GTPases during mesenchymal-to-epithelial-like transitions. Development *145*, dev.157495.

26. Müller, P.M., Rademacher, J., Bagshaw, R.D., Wortmann, C., Barth, C., van Unen, J., Alp, K.M., Giudice, G., Eccles, R.L., Heinrich, L.E., et al. (2020). Systems analysis of RhoGEF and RhoGAP regulatory proteins reveals spatially organized RAC1 signalling from integrin adhesions. Nat. Cell Biol. *22*, 498–511.

27. Zhao, W.M., and Fang, G. (2005). MgcRacGAP controls the assembly of the contractile ring and the initiation of cytokinesis. Proc. Natl. Acad. Sci. USA *102*, 13158–13163.

28. Yüce, O., Piekny, A., and Glotzer, M. (2005). An ECT2-centralspindlin complex regulates the localization and function of RhoA. J. Cell Biol. *170*, 571–582.

29. Mishima, M., Kaitna, S., and Glotzer, M. (2002). Central spindle assembly and cytokinesis require a kinesin-like protein/RhoGAP complex with microtubule bundling activity. Dev. Cell *2*, 41–54.

30. Su, K.C., Takaki, T., and Petronczki, M. (2011). Targeting of the RhoGEF Ect2 to the equatorial membrane controls cleavage furrow formation during cytokinesis. Dev. Cell *21*, 1104–1115.

31. Herszterg, S., Pinheiro, D., and Bellaïche, Y. (2014). A multicellular view of cytokinesis in epithelial tissue. Trends Cell Biol. *24*, 285–293.

32. Ragkousi, K., and Gibson, M.C. (2014). Cell division and the maintenance of epithelial order. J. Cell Biol. *207*, 181–188.

33. Firmino, J., Rocancourt, D., Saadaoui, M., Moreau, C., and Gros, J. (2016). Cell division drives epithelial cell rearrangements during gastrulation in chick. Dev. Cell *36*, 249–261.

34. Gibson, M.C., Patel, A.B., Nagpal, R., and Perrimon, N. (2006). The emergence of geometric order in proliferating metazoan epithelia. Nature *442*, 1038–1041.

35. Higashi, T., Arnold, T.R., Stephenson, R.E., Dinshaw, K.M., and Miller, A.L. (2016). Maintenance of the epithelial barrier and remodeling of cell-cell junctions during cytokinesis. Curr. Biol. *26*, 1829–1842.

36. Herszterg, S., Leibfried, A., Bosveld, F., Martin, C., and Bellaiche, Y. (2013). Interplay between the dividing cell and its neighbors regulates adherens junction formation during cytokinesis in epithelial tissue. Dev. Cell *24*, 256–270.

37. Guillot, C., and Lecuit, T. (2013). Adhesion disengagement uncouples intrinsic and extrinsic forces to drive cytokinesis in epithelial tissues. Dev. Cell *24*, 227–241.

38. Founounou, N., Loyer, N., and Le Borgne, R. (2013). Septins regulate the contractility of the actomyosin ring to enable adherens junction remodeling during cytokinesis of epithelial cells. Dev. Cell *24*, 242–255.

39. Morais-De-Sá, E., and Sunkel, C. (2013). Adherens junctions determine the apical position of the midbody during follicular epithelial cell division. EMBO Rep. *14*, 696–703.

40. McKinley, K.L., Stuurman, N., Royer, L.A., Schartner, C., Castillo-Azofeifa, D., Delling, M., Klein, O.D., and Vale, R.D. (2018). Cellular aspect ratio and cell division mechanics underlie the patterning of cell progeny in diverse mammalian epithelia. Elife *7*, e36739.

41. Lau, K., Tao, H., Liu, H., Wen, J., Sturgeon, K., Sorfazlian, N., Lazic, S., Burrows, J.T.A.A., Wong, M.D., Li, D., et al. (2015). Anisotropic stress orients remodelling of mammalian limb bud ectoderm. Nat. Cell Biol. *17*, 569–579.

42. Pinheiro, D., Hannezo, E., Herszterg, S., Bosveld, F., Gaugue, I., Balakireva, M., Wang, Z., Cristo, I., Rigaud, S.U., Markova, O., and Bellaïche, Y. (2017). Transmission of cytokinesis forces via E-cadherin dilution and actomyosin flows. Nature *545*, 103–107.

43. Duhart, J.C., Parsons, T.T., and Raftery, L.A. (2017). The repertoire of epithelial morphogenesis on display: progressive elaboration of *Drosophila* egg structure. Mech. Dev. *148*, 18–39.

44. Wang, Z., Bosveld, F., and Bellaïche, Y. (2018). Tricellular junction proteins promote disentanglement of daughter and neighbour cells during epithelial cytokinesis. J. Cell Sci. *131*, jcs215764.

45. Daniel, E., Daudé, M., Kolotuev, I., Charish, K., Auld, V., and Le Borgne, R. (2018). Coordination of septate junctions assembly and completion of cytokinesis in proliferative epithelial tissues. Curr. Biol. *28*, 1380–1391.e4.

46. Guirao, B., Rigaud, S.U., Bosveld, F., Bailles, A., López-Gay, J., Ishihara, S., Sugimura, K., Graner, F., and Bellaïche, Y. (2015). Unified quantitative characterization of epithelial tissue development. Elife *4*, e08519.

47. Chen, D.Y., Crest, J., Streichan, S.J., and Bilder, D. (2019). Extracellular matrix stiffness cues junctional remodeling for 3D tissue elongation. Nat. Commun. *10*, 3339.

48. Dent, L.G., Manning, S.A., Kroeger, B., Williams, A.M., Saiful Hilmi, A.J., Crea, L., Kondo, S., Horne-Badovinac, S., and Harvey, K.F. (2019). The dPix-Git complex is essential to coordinate epithelial morphogenesis and regulate myosin during Drosophila egg chamber development. PLoS Genet. *15*, e1008083.

49. Neisch, A.L., Formstecher, E., and Fehon, R.G. (2013). Conundrum, an ARHGAP18 orthologue, regulates RhoA and proliferation through interactions with Moesin. Mol. Biol. Cell *24*, 1420–1433.

50. Prokopenko, S.N., Saint, R., and Bellen, H.J. (2000). Tissue distribution of PEBBLE RNA and pebble protein during Drosophila embryonic development. Mech. Dev. *90*, 269–273.

51. Jones, W.M., Chao, A.T., Zavortink, M., Saint, R., and Bejsovec, A. (2010). Cytokinesis proteins Tum and Pav have a nuclear role in Wnt regulation. J. Cell Sci. *123*, 2179–2189.

52. Schmidt, A., Lv, Z., and Großhans, J. (2018). Elmo and sponge specify subapical restriction of canoe and formation of the subapical domain in early Drosophila embryos. Development *145*, dev157909.

53. Ramkumar, N., and Baum, B. (2016). Coupling changes in cell shape to chromosome segregation. Nat. Rev. Mol. Cell Biol. *17*, 511–521.

54. Rosa, A., Vlassaks, E., Pichaud, F., and Baum, B. (2015). Ect2/Pbl acts via Rho and polarity proteins to direct the assembly of an isotropic actomyosin cortex upon mitotic entry. Dev. Cell *32*, 604–616.

55. Aguilar-Aragon, M., Bonello, T.T., Bell, G.P., Fletcher, G.C., and Thompson, B.J. (2020). Adherens junction remodelling during mitotic rounding of pseudostratified epithelial cells. EMBO Rep. *21*, e49700.

56. Airoldi, S.J., McLean, P.F., Shimada, Y., and Cooley, L. (2011). Intercellular protein movement in syncytial Drosophila follicle cells. J. Cell Sci. *124*, 4077–4086.

57. Chaigne, A., and Brunet, T. (2022). Incomplete abscission and cytoplasmic bridges in the evolution of eukaryotic multicellularity. Curr. Biol. *32*, R385–R397.

58. Acharya, B.R., Nestor-Bergmann, A., Liang, X., Gupta, S., Duszyc, K., Gauquelin, E., Gomez, G.A., Budnar, S., Marcq, P., Jensen, O.E., et al. (2018). A mechanosensitive RhoA pathway that protects epithelia against acute tensile stress. Dev. Cell *47*, 439–452.e6.

59. Duszyc, K., Gomez, G.A., Lagendijk, A.K., Yau, M.K., Nanavati, B.N., Gliddon, B.L., Hall, T.E., Verma, S., Hogan, B.M., Pitson, S.M., et al. (2021). Mechanotransduction activates RhoA in the neighbors of apoptotic epithelial cells to engage apical extrusion. Curr. Biol. *31*, 1326–1336.e5.

60. Munjal, A., Philippe, J.M., Munro, E., and Lecuit, T. (2015). A self-organized biomechanical network drives shape changes during tissue morphogenesis. Nature *524*, 351–355.

61. Lee, S., Park, H., Kyung, T., Kim, N.Y., Kim, S., Kim, J., and Heo, W.D. (2014). Reversible protein inactivation by optogenetic trapping in cells. Nat. Methods *11*, 633–636.

62. Qin, X., Park, B.O., Liu, J., Chen, B., Choesmel-Cadamuro, V., Belguise, K., Heo, W.D., and Wang, X. (2017). Cell-matrix adhesion and cell-cell adhesion differentially control basal myosin oscillation and Drosophila egg chamber elongation. Nat. Commun. *8*, 14708.

63. Delague, V., Jacquier, A., Hamadouche, T., Poitelon, Y., Baudot, C., Boccaccio, I., Chouery, E., Chaouch, M., Kassouri, N., Jabbour, R., et al. (2007). Mutations in FGD4 encoding the Rho GDP/GTP exchange factor FRABIN cause autosomal recessive Charcot-Marie-Tooth type 4H. Am. J. Hum. Genet. *81*, 1–16.

64. Renda, I., Bianchi, S., Vezzosi, V., Nori, J., Vanzi, E., Tavella, K., and Susini, T. (2019). Expression of FGD3 gene as prognostic factor in young breast cancer patients. Sci. Rep. *9*, 15204.

65. Nahm, M., Lee, M., Baek, S.H., Yoon, J.H., Kim, H.H., Lee, Z.H., and Lee, S. (2006). Drosophila RhoGEF4 encodes a novel RhoA-specific guanine exchange factor that is highly expressed in the embryonic central nervous system. Gene *384*, 139–144.

66. Abreu-Blanco, M.T., Verboon, J.M., and Parkhurst, S.M. (2014). Coordination of rho family GTPase activities to orchestrate cytoskeleton responses during cell wound repair. Curr. Biol. *24*, 144–155.

67. Georgiou, M., and Baum, B. (2010). Polarity proteins and Rho GTPases cooperate to spatially organise epithelial actin-based protrusions. J. Cell Sci. *123*, 1089–1098.

68. Aigouy, B., Farhadifar, R., Staple, D.B., Sagner, A., Röper, J.C., Jülicher, F., and Eaton, S. (2010). Cell flow reorients the axis of planar polarity in the wing epithelium of drosophila. Cell *142*, 773–786.

69. Uroz, M., Wistorf, S., Serra-Picamal, X., Conte, V., Sales-Pardo, M., Roca-Cusachs, P., Guimerà, R., and Trepat, X. (2018). Regulation of cell cycle progression by cell–cell and cell–matrix forces. Nat. Cell Biol. *20*, 646–654.

70. Ninov, N., Manjón, C., and Martín-Blanco, E. (2009). Dynamic control of cell cycle and growth coupling by ecdysone, egfr, and PI3K signaling in Drosophila histoblasts. PLOS Biol. *7*, e1000079.

71. Davis, J.R., Ainslie, A.P., Williamson, J.J., Ferreira, A., Torres-Sánchez, A., Hoppe, A., Mangione, F., Smith, M.B., Martin-Blanco, E., Salbreux, G., and Tapon, N. (2022). ECM degradation in the Drosophila abdominal epidermis initiates tissue growth that ceases with rapid cell-cycle exit. Curr. Biol. *32*, 1285–1300.e4.

72. Bischoff, M., and Cseresnyés, Z. (2009). Cell rearrangements, cell divisions and cell death in a migrating epithelial sheet in the abdomen of Drosophila. Development *136*, 2403–2411.

73. Sugimura, K., and Ishihara, S. (2013). The mechanical anisotropy in a tissue promotes ordering in hexagonal cell packing. Development *140*, 4091–4101.

74. Fernandez-Gonzalez, R., and Peifer, M. (2022). Powering morphogenesis: multiscale challenges at the interface of cell adhesion and the cytoskeleton. Mol. Biol. Cell *33*.

75. Monster, J.L., Donker, L., Vliem, M.J., Win, Z., Matthews, H.K., Cheah, J.S., Yamada, S., de Rooij, J., Baum, B., and Gloerich, M. (2021). An asymmetric junctional mechanoresponse coordinates mitotic rounding with epithelial integrity. J. Cell Biol. *220*, e202001042.

76. Pinheiro, D., and Bellaïche, Y. (2018). Mechanical force-driven adherens junction remodeling and epithelial dynamics. Dev. Cell *47*, 3–19.

77. Priya, R., Gomez, G.A., Budnar, S., Verma, S., Cox, H.L., Hamilton, N.A., and Yap, A.S. (2015). Feedback regulation through myosin II confers robustness on RhoA signalling at E-cadherin junctions. Nat. Cell Biol. *17*, 1282–1293.

78. Simões, S., Lerchbaumer, G., Pellikka, M., Giannatou, P., Lam, T., Kim, D., Yu, J., Stal, D. Ter, Al Kakouni, K., Fernandez-Gonzalez, R., and Tepass, U. (2022). Crumbs complex–directed apical membrane dynamics in epithelial cell ingression. J. Cell Biol. *221*, e202108076.

79. Lecuit, T., and Yap, A.S. (2015). E-cadherin junctions as active mechanical integrators in tissue dynamics. Nat. Cell Biol. *17*, 533–539.

80. Chu, Y.S., Thomas, W.A., Eder, O., Pincet, F., Perez, E., Thiery, J.P., and Dufour, S. (2004). Force measurements in E-cadherin-mediated cell doublets reveal rapid adhesion strengthened by actin cytoskeleton remodeling through Rac and Cdc42. J. Cell Biol. *167*, 1183–1194.

81. Verma, S., Han, S.P., Michael, M., Gomez, G.A., Yang, Z., Teasdale, R.D., Ratheesh, A., Kovacs, E.M., Ali, R.G., and Yap, A.S. (2012). A WAVE2-Arp2/3 actin nucleator apparatus supports junctional tension at the epithelial zonula adherens. Mol. Biol. Cell *23*, 4601–4610.

82. Yamada, S., and Nelson, W.J. (2007). Localized zones of Rho and Rac activities drive initiation and expansion of epithelial cell-cell adhesion. J. Cell Biol. *178*, 517–527.

83. Loria, A., Longhini, K.M., and Glotzer, M. (2012). The RhoGAP domain of CYK-4 Has an essential role in RhoA activation. Curr. Biol. *22*, 213–219.

84. McGuire, S.E., Le, P.T., and Davis, R.L. (2001). The role of Drosophila mushroom body signaling in olfactory memory. Science *293*, 1330–1333.

85. Bosveld, F., Ainslie, A., and Bellaïche, Y. (2017). Sequential activities of Dynein, Mud and Asp in centrosome-spindle coupling maintain centrosome number upon mitosis. J. Cell Sci. *130*, 3557–3567.

86. Huang, J., Zhou, W., Dong, W., Watson, A.M., and Hong, Y. (2009). From the cover: directed, efficient, and versatile modifications of the Drosophila genome by genomic engineering. Proc. Natl. Acad. Sci. USA *106*, 8284–8289.

87. López-Gay, J.M., Nunley, H., Spencer, M., di Pietro, F., Guirao, B., Bosveld, F., Markova, O., Gaugue, I., Pelletier, S., Lubensky, D.K., and Bellaïche, Y. (2020). Apical stress fibers enable a scaling between cell mechanical response and area in epithelial tissue. Science *370*, eabb2169.

88. Rauzi, M., Lenne, P.F., and Lecuit, T. (2010). Planar polarized actomyosin contractile flows control epithelial junction remodelling. Nature *468*, 1110–1114.

89. Ambrosini, A., Rayer, M., Monier, B., and Suzanne, M. (2019). Mechanical function of the nucleus in force generation during epithelial morphogenesis. Dev. Cell *50*, 197–211.e5.

90. Conduit, P.T., Feng, Z., Richens, J.H., Baumbach, J., Wainman, A., Bakshi, S.D., Dobbelaere, J., Johnson, S., Lea, S.M., and Raff, J.W. (2014). The centrosome-specific phosphorylation of Cnn by Polo/Plk1 drives Cnn scaffold assembly and centrosome maturation. Dev. Cell *28*, 659–669.

91. Strutt, D.I., Weber, U., and Mlodzik, M. (1997). The role of RhoA in tissue polarity and Frizzled signalling. Nature *387*, 292–295.

92. Dietzl, G., Chen, D., Schnorrer, F., Su, K.C., Barinova, Y., Fellner, M., Gasser, B., Kinsey, K., Oppel, S., Scheiblauer, S., et al. (2007). A genome-wide transgenic RNAi library for conditional gene inactivation in Drosophila. Nature *448*, 151–156.

93. Li, M.Z., and Elledge, S.J. (2012). SLIC: a method for sequence- and ligation-independent cloning. Methods Mol. Biol. *852*, 51–59.

94. Venken, K.J.T., Carlson, J.W., Schulze, K.L., Pan, H., He, Y., Spokony, R., Wan, K.H., Koriabine, M., de Jong, P.J., White, K.P., et al. (2009). Versatile P[acman] BAC libraries for transgenesis studies in Drosophila melanogaster. Nat. Methods *6*, 431–434.

95. Venken, K.J.T., Kasprowicz, J., Kuenen, S., Yan, J., Hassan, B.A., and Verstreken, P. (2008). Recombineering-mediated tagging of Drosophila genomic constructs for in vivo localization and acute protein inactivation. Nucleic Acids Res. *36*, e114.

96. Port, F., Chen, H.M., Lee, T., and Bullock, S.L. (2014). Optimized CRISPR/Cas tools for efficient germline and somatic genome engineering in Drosophila. Proc. Natl. Acad. Sci. USA *111*, E2967–E2976.

97. Kanca, O., Zirin, J., Garcia-Marques, J., Knight, S.M., Yang-Zhou, D., Amador, G., Chung, H., Zuo, Z., Ma, L., He, Y., et al. (2019). An efficient CRISPR-based strategy to insert small and large fragments of DNA using short homology arms. Elife *8*, e51539.

98. Gratz, S.J., Ukken, F.P., Rubinstein, C.D., Thiede, G., Donohue, L.K., Cummings, A.M., and O'Connor-Giles, K.M. (2014). Highly specific and efficient CRISPR/Cas9-catalyzed homology-directed repair in Drosophila. Genetics *196*, 961–971.

99. Huang, J., Zhou, W., Watson, A.M., Jan, Y.N., and Hong, Y. (2008). Efficient ends-out gene targeting in drosophila. Genetics *180*, 703–707.

100. Massarwa, R., Schejter, E.D., and Shilo, B.Z. (2009). Apical secretion in epithelial tubes of the drosophila embryo is directed by the Formin-family protein Diaphanous. Dev. Cell *16*, 877–888.

101. Simões, S., Denholm, B., Azevedo, D., Sotillos, S., Martin, P., Skaer, H., Hombría, J.C.G., and Jacinto, A. (2006). Compartmentalisation of Rho regulators directs cell invagination during tissue morphogenesis. Development *133*, 4257–4267.

102. Sotillos, S., Aguilar-Aragon, M., and Hombría, J.C. (2018). Functional analysis of the Drosophila RhoGAP Cv-c protein and its equivalence to the human DLC3 and DLC1 proteins. Sci. Rep. *8*, 4601.

103. Zhang, X., Koolhaas, W.H., and Schnorrer, F. (2014). A versatile two-step CRISPR- and RMCE-based strategy for efficient genome engineering in Drosophila. G3 (Bethesda) *4*, 2409–2418.

104. Brand, A.H., and Perrimon, N. (1993). Targeted gene expression as a means of altering cell fates and generating dominant phenotypes. Development *118*, 401–415.

105. McGuire, S.E., Le, P.T., Osborn, A.J., Matsumoto, K., and Davis, R.L. (2003). Spatiotemporal rescue of memory dysfunction in drosophila. Science *302*, 1765–1768.

106. Golic, K.G., and Lindquist, S. (1989). The FLP recombinase of yeast catalyzes site-specific recombination in the Drosophila genome. Cell *59*, 499–509.

107. Bosveld, F., Bonnet, I., Guirao, B., Tlili, S., Wang, Z., Petitalot, A., Marchand, R., Bardet, P.L., Marcq, P., Graner, F., and Bellaïche, Y. (2012). Mechanical control of morphogenesis by fat/Dachsous/Four-jointed planar cell polarity pathway. Science *336*, 724–727.

108. Bardet, P.L., Guirao, B., Paoletti, C., Serman, F., Léopold, V., Bosveld, F., Goya, Y., Bosveld, F., Graner, F., and Bellaïche, Y. (2013). PTEN controls junction lengthening and stability during cell rearrangement in epithelial tissue. Dev. Cell *25*, 534–546.

109. Osswald, M., Barros-Carvalho, A., Carmo, A.M., Loyer, N., Gracio, P.C., Sunkel, C.E., Homem, C.C.F., Januschke, J., and Morais-de-Sá, E. (2022). aPKC regulates apical constriction to prevent tissue rupture in the Drosophila follicular epithelium. Curr. Biol. *32*, 4411–4427.e8.

110. Heller, D., Hoppe, A., Restrepo, S., Gatti, L., Tournier, A.L., Tapon, N., Basler, K., and Mao, Y. (2016). EpiTools: an open-source image analysis toolkit for quantifying epithelial growth dynamics. Dev. Cell *36*, 103–116.

111. Olmos, Y., Perdrix-Rosell, A., and Carlton, J.G. (2016). Membrane binding by CHMP7 coordinates ESCRT-III-dependent nuclear envelope reformation. Curr. Biol. *26*, 2635–2641.

STAR★METHODS

KEY RESOURCES TABLE

REAGENT or RESOURCE	SOURCE	IDENTIFIER
Experimental models: Organisms/strains		
Drosophila: Act5C-Gal4	Bloomington Drosophila Stock Center.	BDSC#3954
Drosophila: tub-Gal80^{ts}	McGuire et al.[84]; Bloomington Drosophila Stock Center	BDSC#7017
Drosophila : Act5c>cd2>GAL4	Bloomington Drosophila Stock Center	BDSC#4780
Drosophila: hs-flp	Bloomington Drosophila Stock Center	
Drosophila: FRT80B, nls:GFP	Bloomington Drosophila Stock Center	BDSC #5630
Drosophila: FRT80B, H2A:RFP	Bloomington Drosophila Stock Center	BDSC#34499
Drosophila: FRT40A, nls:GFP	Bloomington Drosophila Stock Center	BDSC#5629
Drosophila: FRT40A, ubi-H2B:RFP	Bosveld et al.[85]	NA
Drosophila:Cyo,hs-Cre	Bloomington Drosophila Stock Center	BDSC#1092
Drosophila:TM6,hs-Cre	Bloomington Drosophila Stock Center	BDSC#1501
Drosophila: Ecad:GFP^{ki}	Huang et al.[86]; gift of Yang Hong	NA
Drosophila: Ecad:3xmKate2	Pinheiro et al.[34]	NA
Drosophila: sqh:3xmKate2	Pinheiro et al.[34]	NA
Drosophila: sqh:3xGFP	Pinheiro et al.[34]	NA
Drosophila: UAS-CAAX:tBFP (II)	López-Gay et al.[87]	NA
Drosophila: UAS-CAAX:tBFP (III)	López-Gay et al.[87]	NA
Drosophila: UAS-LARIAT	Qin et al.[62]	NA
Drosophila: sqh-Utr:ABD:GFP	Rauzi et al.[88]	NA
Drosophila: ubi-PLCgPH:GFP	Gift from F. Pichaud	NA
Drosophila: ubi-PLCgPH:chFP	Herszterg et al.[36]	NA
Drosophila: ubi-Anillin-Rho binding Domain:GFP	Munjal et al.,[60] gift from T. Lecuit	NA
Drosophila: Rac1:GFP	Bloomington Drosophila Stock Center	BDSC#52284
Drosophila: sqh-Pak3-RhoGTPases Binding Domain: GFP	Bloomington Drosophila Stock Center	BDSC#52303
Drosophila: Scar:GFP	This study	NA
Drosophila: Lamin:TagRFP^{ki}	Ambrosini et al.,[89] gift from M.Suzanne	NA
Drosophila: Nup107:RFP	Bloomington Drosophila Stock Center	BDSC#35517
Drosophila: ubi-Spd2:RFP	Conduit et al.[90]	NA
Drosophila: *rhogef4*$^{\Delta RMCE}$	This study	NA
Drosophila: *cysts*$^{\Delta RMCE}$	This study	NA
Drosophila: FRT *Rho1*^{72M1}	Strutt et al.[91]	NA
Drosophila: Df (3L) BSC117	Bloomington Drosophila Stock Center	BDSC#8974
Drosophila: UAS-pnut^{dsRNA}	VDRC Stock Center, Dietzl et al.[92]	VDRC#11791
Drosophila: UAS-shg^{dsRNA}	VDRC Stock Center, Dietzl et al.[92]	VDRC#27082
Drosophila: UAS-Rok^{dsRNA}	Bloomington Drosophila Stock Center	BDSC28797
Drosophila: vas-cas9	Bloomington Drosophila Stock Center.	BDSC#55821
Drosophila: vas-cas9	Bloomington Drosophila Stock Center.	BDSC#51324
Drosophila: fluorescently tagged RhoGEF/ GAP	This study, see Methods S1.	
Oligonucleotides		
See Methods S1		

(*Continued on next page*)

Continued		
REAGENT or RESOURCE	SOURCE	IDENTIFIER
Recombinant DNA		
See Methods S1		
Chemicals		
Insulin solution from bovine pancreas	Sigma-Aldrich	Cat# I0516
Schneider's Insect Medium	Sigma-Aldrich	Cat# S0146
Cell Mask Orange Plasma membrane Stain	ThermoFisher	Cat# C10045
Software and algorithms		
Fiji	http://fiji.sc	SCR_002285
MetaMorph Microscopy Automation and Image Analysis Software	Molecular devices http://www.moleculardevices.com/Products/Software/Meta-Imaging-Series/MetaMorph.html	SCR_002368
ZEN Digital Imaging for Light Microscopy	Zeiss http://www.zeiss.com/microscopy/en_us/products/microscope-software/zen.html#introduction	SCR_013672
Graphpad Prism	Graphpad software http://www.graphpad.com/	SCR_002798
Matlab	Mathworks http://www.mathworks.com/products/matlab/	SCR_001622

RESOURCE AVAILABILITY

Lead contact

Further information and requests for resources and reagents should be directed to, and will be fulfilled by the lead contact, Yohanns Bellaïche (yohanns.bellaiche@curie.fr).

Materials availability

All unique/stable reagents generated in this study are available from the lead contact without restriction.

Data and code availability

- All original microscopy data reported in this paper will be shared by the lead contact upon request.
- This paper does not report original code.
- Any additional information required to reanalyze the data reported in this paper is available from the lead contact upon request.

EXPERIMENTAL MODEL AND SUBJECT DETAILS

Fly husbandry and stocks

Flies were grown on standard molasses/cornmeal/yeast food at 18°C or 25°C, and experiments were performed at 25° unless otherwise specified. Drosophila melanogaster stocks used in this study and associated references are listed in the key resources table.

METHOD DETAILS

Molecular Biology and Transgenesis

Methods S1 lists BAC and plasmids generated in this study, their parental BAC or plasmids, as well as the oligonucleotides used. Oligonucleotides were bought from Sigma. Cloning was performed by primer annealing and ligation, or by sequence- and ligation-independent cloning SLIC.[93] All regions amplified by PCR as well as junctions between tag and genomic sequences were checked by sequencing. Transgenesis was performed by BestGene or Rainbow transgenesis services.

Transgenic Fluorescently tagged RhoGEF/GAP Library

Recombineering based Tagging

To create the GFP-tagged transgenes of CG15611, CG43658, RhoGEF2, RtGEF, Trio, RacGAP84C, RhoGAP100F, RhoGAP102A and RhoGAP93B expressed under the control of their endogenous promoter, we used recombineering[94] to introduce an in-frame GFP sequence in N- or C-term of the open reading frame in BAC genomic clones (see Methods S1A and S1B for GFP position, tagged isoforms and BAC clones from the BACPAC Resources Center[94]). To insert a GFP sequence at the amino acid positions indicated in Methods S1A and S1B by recombineering, a GFP sequence and a neomycin resistance cassette flanked by loxP sites and homologous sequences were amplified by PCR and recombined in each BAC.[95] Upon neomycin selection, the cassette was removed by Cre-mediated recombination leaving behind a 78 bp loxP site sequence. Each GFP insertion was verified by sequencing. Each BAC construct was integrated at the PBac{y[+]-attP-9A}VK00033 landing site at 65B2 and their genomic insertion was confirmed by PCR and sequencing.

CRISPR/Cas9 mediated tagging

The remaining RhoGEF/GAP were tagged with either GFP or mKate2 at their endogenous locus using CRISPR/Cas9 mediated homologous recombination.[96,97] To generate the tagged alleles by CRISPR/Cas9-mediated homologous recombination, guide RNA sequences were selected using CRISPR Optimal Target Finder (http://targetfinder.flycrispr.neuro.brown.edu/index.php)[98], and corresponding oligonucleotides were cloned into the pCFD5 (Addgene #73914) or pCFD3-dU6:3gRNA (Addgene #49410) guide vectors (Methods S1A and S1B). Homology sequences were cloned into homologous recombination vectors harbouring a *hs-mini-white* cassette flanked by two loxP sites[42,99] and an N- or C-terminal GFP or mKate2 sequences using the pCRISPR-GFP-Nter, pCRISPR-GFP-Cter, pCRISPR-mKate-Nter and pCRISPR-mKate-Cter vectors.[42] The two homologous regions were cloned using the primers indicated in Methods S1A and S1B. Plasmids expressing the guide RNAs for each RhoGEF/GAP tagging were co-injected in *vas-cas9* embryos. When injecting donors for RhoGEF/GAP for which both the mKate2 and GFP donor plasmids were cloned, we co-injected GFP and mKate2 donor plasmids at a 2/3 and 1/3 ratio to favour GFP tagging. Upon excision of the *mini-white* (*mw*) transgenesis marker using hs-Cre lines on chromosome II or III, each fluorescently tagged allele was verified by sequencing. Five out of 39 CRISPR/Cas9 line are homozygote lethal. Their lethality likely stems from the lowered level of RhoGEF/GAP activity upon GFP tagging. The endogenous localizations of RhoGEF64C,[100,101] Spg[100]; RhoGAP71E[21] and Cv-c[102] have been previously reported in other epithelial tissues in interphase using GFP-tagged versions, antibody or MiMIC lines. For RhoGEF64C, Spg and RhoGAP71E, using our corresponding CRISPR/Cas9 lines, we observed localizations similar to the ones previously reported. For Cv-c, using our CRISPR/Cas9 line, we observed a weak apical junctional localization in the notum, and a basolateral enrichment in the larval salivary glands, as reported for the embryonic ones.[102] We have generated BAC and CRISPR/Cas9 lines for RhoGEF3 and RhoGAP15B. For both RhoGEF3 and RhoGAP15B, we have observed similar localization when using their respective BAC or CRISPR/Cas9 lines (see website).

Plasmid Library for generating RhoGEF/GAP deletion RMCE alleles

To facilitate the generation of loss of function alleles of each RhoGEF/GAP using CRISPR/Cas9 mediated homologous recombination, we generated a plasmid library of guide and donor plasmids to replace most of each RhoGEF/GAP coding region by a *mw* gene flanked by 2 attP Phi31 recombination sites (See Methods S1C and S1D for guide and donor plasmids and deletions positions) using the pCRISPR-del[42] or pCRISPR-del-HighThrouput[97] plasmids. Using the well-established approach known as RMCE based on the φ31 recombinase[103] (Figure S1B), one can then efficiently replace the *mini-white* gene by any DNA sequence to perform structure-function analysis or tagging with any fluorescent or non-fluorescent tags (Figure S1B). The plasmid library was used to generate $cyst^{\Delta RMCE}$ and $rhogef4^{\Delta RMCE}$ null alleles. $cyst^{\Delta RMCE}$ is associated with a deletion of the *cysts* reading frame from G233 to F1309 (numbered according to the isoform RA, 1309 aa) and $rhogef4^{\Delta RMCE}$ deletes from M1 to F647 (numbered according to the isoform RA, 647 aa) of the *rhogef4* reading frame.

Genetics, somatic clones and RNA interference

Both female and male animals were used in experiments in the pupa, except in Figure 3A for which females were used; adult females were used for experiments in the FE. Experiments using the Gal4/UAS, the Gal4/$Gal80^{ts}$/UAS systems,[104,105] hs-FLP induced FLPout clones and FRT site mitotic recombination[106] were done as previously described.[107] $cyst^{\Delta RMCE}$, $rhogef4^{\Delta RMCE}$, $Rho1^{72M1}$, Cysts:GFP, Ani-RBD:GFP, PH:GFP/chFP, and GFP:RhoGEF4 somatic clones were generated by FRT/FLP induced mitotic recombination, and mutant cells were marked by the loss of fluorescent markers. Clones in the pupa were generated via a 45min-1h heat-shock at 37°C 3-4 days before live-imaging. Clones in the FE were induced via heat-shocking 2 times for 2h at 37°C 2-5 days before imaging. The *cysts,rhogef4* double mutant cells were obtained by inducing $cyst^{\Delta RMCE}$ clones in $rhogef4^{\Delta RMCE}$ mutant animals. Experiments in the pupal wing (Figures S7B and S7D) were performed using the $rhogef4^{\Delta RMCE}$/Df(3L)BSC117 genotype; Df(3L) deletes the *rhogef4* locus. Experiments in Figures S5D, S5E, and S6F were done in ovaries dissected from $rhogef4^{\Delta RMCE}$ homozygous flies expressing Ecad:GFP and MyoII:3xmKate2, and Ecad:GFP, MyoII:3xmKate2 flies were used as control.

The $pnut^{RNAi}$, $ecad^{RNAi}$ *or* rok^{RNAi} clones were generated by driving the expression of *UAS-*$pnut^{dsRNA}$, *UAS-*$ecad^{dsRNA}$ or *UAS-*rok^{dsRNA}, respectively, using hs-FLP induced flp-out on the Act>Cdc2>Gal4, UAS-CAAX:tBFP line to express Gal4 and label the clones by membrane localized tBFP.

Pupa and egg chamber mounting for imaging

Pupae were collected and mounted for dorsal thorax, wing or histoblast live imaging as described previously.[42,107,108] Dissected egg chambers were imaged live in culture medium (Schneider's medium, Sigma-Aldrich) supplemented with 10% Fetal bovine serum (Thermo Fisher) and 200 μg/uL insulin (Sigma-Aldrich) as previously described.[109] For imaging of fixed tissue, egg chambers were fixed in 4% paraformaldehyde solution in PBT (PBS + 0.2% Tween 20, Sigma-Aldrich) for 20 min, washed with PBT and mounted with Vectashield with DAPI (Vector Laboratories).

Microscopy

Microscopes, software and imaging: Samples were imaged at 25°C, unless otherwise specified.

Imaging of pupal tissues

The imaging was performed on: (i) an inverted confocal spinning disk microscope CSU-W1 (Andor/Roper/Nikon) equipped with a sCMOS camera (Flash4 Hamamatsu), and a Borealis module from Andor for better field homogeneity, using either a 60x (NA1.4 OIL PL APO L) or 100x (NA1.45 OIL PL APO L); (ii) an inverted confocal spinning disk microscope from Zeiss (CSUW1, Roper/Zeiss) equipped with a sCMOS camera (Flash4 Hamamatsu), a Visitron module for better field homogeneity, using either 60x or 100x NA1.4 OIL DIC N2 PL APO VC objectives; (iii) an inverted spinning disk wide confocal microscope CSU-W1 (Roper/Nikon/GATACA) equipped with a sCMOS camera (BSI camera), a field illumination homogenizer, using either 60x or 100X (NA 1.4 OIL N2 PL APO VC) objectives. The Metamorph autofocus function was used for some time-lapse acquisitions.

Imaging of egg chambers

The imaging was done on either: (i) an Andor XD Revolution Spinning Disk Confocal system (Yokogawa CSU-22 unit) equipped with two solid state lasers (488nm and 561nm), an iXonEM+ DU-897 EMCCD camera, and built on an inverted Olympus IX81 microscope with a 60x (NA1.42 OIL PLAPON) or a 100x (NA1.40 OIL UPLSAPO) objective using iQ software (Andor); (ii) an inverted laser scanning confocal microscope Leica SP8 (Leica Microsystems) with a 63x (NA1.30 GLYCEROL) objective; (iii) an inverted laser scanning confocal microscope Leica TCS SP5 II (Leica Microsystems) with a 63x (NA1.3 GLYCEROL) objective.

Localization screen of tagged RhoGEF/GAPs in epithelial tissues

To determine the localization of GFP-tagged RhoGEF/GAPs in living epithelial notum tissue, a series of sequential acquisitions were performed for each tagged protein. First, using MyoII:3xmKate2 as a reference, the GFP signal was imaged at different apical-basal levels both in interphase and dividing cells. Following this initial imaging, two complementary acquisitions were used to better capture each RhoGEF/GAP localization or resolve their dynamics at a relevant position along the apical-basal axis: i) a single z-stack acquisition at high laser power for RhoGEF/GAPs expressed at intermediate/low levels; ii) a z-stack and time-lapse serie using a time interval ranging from 30s to 4min, adjusted to reduce bleaching of the GFP signal, and to image cell division. In both cases, the apical and basal positions of the z-stack acquisitions were set to the relevant z-plans as determined by the initial observations.

The localizations of fluorescently tagged RhoGEF/GAPs were determined in live and fixed egg chambers through the acquisitions of z-stacks (z-step between 0.5 and 1 μm): (i) at the surface of the egg chamber to cross-section the FE along the apical-basal axis (labelled as "xy" in figures); (ii) along the midsagittal region of the egg chamber, which enables the visualization of the whole apical-basal axis of the epithelium in a confocal section plane (labelled as "yz" in figures). MyoII:3xmKate2 or CellMask Orange Plasma membrane Stain (ThermoFisher; C10045; diluted 1:10 000 in *ex vivo* culture medium (Schneider's medium (Sigma-Aldrich) supplemented with 10% Fetal bovine serum (Thermo Fisher) and 200 μg/uL insulin (Sigma-Aldrich) and washed twice with *ex vivo* culture medium before imaging) were used to label the actomyosin cytoskeleton or the plasma membrane, respectively, to resolve the fluorescently tagged RhoGEF/GAP position along the apical-basal axis.

Optogenetics

Experimental crosses were protected from light by wrapping the Drosophila tubes into an aluminium foil and were grown at 18°C. White pupae (0 hAPF) were selected under white light, and then kept in the dark until the experiment performed at 29°C to induce the expression of the LARIAT transgene. Pupae were mounted under amber light (white light lamp source equipped with a 630/692nm BrightLine® single-band bandpass filter) in a dark room to avoid LARIAT activation. Photoactivation of LARIAT was achieved using repeated illumination (6 0.5μm z-section every 30 sec) with a 488nm laser set at 20-50% of its maximal power on a spinning disk microscope. This routine was selected as it promotes efficient Ecad:GFP clustering at the AJ.

Laser ablation of the cytokinetic ring

To ablate the cytokinetic ring, an inverted confocal microscope from Carl Zeiss (LSM880 NLO) equipped with a two photon laser Ti:Sapphire laser (Mai Tai DeepSee, Spectra Physics) was used. Cells were imaged in monophoton using the 488nm and 561nm lasers with a 40x objective NA1.3 OIL DICII PL APO (optical zoom 3x) at the level of the AJ using MyoII:3xmKate2 and Cysts:GFP to follow both the cytokinetic ring constriction and Cysts dynamics. The ablation was performed at or after mid ring contraction in a region of interest (ROI) encompassing most of apical cytokinetic ring and excluding the ingression membrane to avoid ablating MyoII and Cysts flows. The ablation was done by scanning the ROI at the level of the apical cytokinetic ring using the multiphoton laser set at 810 nm and 13% of its maximal power. Upon ablation, MyoII:3xmKate and Cysts:GFP time-lapse images were acquired. The ablation led to apical relaxation confirming the ablation of the ring and the decrease of ring contractile forces.

QUANTIFICATION AND STATISTICAL ANALYSIS

Quantifications were performed using the Fiji software and a set of home-made macros.

Dynamics of cytokinesis, membrane juxtaposition and AJ formation

Constriction rate and time of 80% contraction

The rates of constriction were determined as previously described.[36] Briefly, the speed of cytokinetic ring constriction in the plane of the AJ was used as a proxy of the cytokinetic constriction rate on MyoII:3xmKate2 and Ecad:GFP confocal time lapse images. To determine constriction rate and the time-point corresponding to 80% of constriction, manual measurements of the initial apical cell length at the site of ring formation, and of the length of apical contractile ring were performed using a home-made Fiji macro. The rate of constriction was determined as the slope of the linear fit of the contractile ring length, normalized to its initial apical length at the onset of cytokinesis, as a function of time.[36]

Angle formed by the ingressing AJ

In control and mutant conditions, the angle (from 0° to 90°) formed by the ingressing AJ was quantified in time-lapse movies of Ecad:GFP and MyoII:3xmKate2, as schematically represented in Figure 3D; a 0° angle corresponds to maximal daughter cell membrane juxtaposition. The angles were measured manually at 80% of constriction of the dividing cell using a Fiji Macro as previously done.[42]

Junction formation dynamics in the notum

The timing and the initial length of the *de novo* AJ formed upon division were determined in Ecad:GFP and MyoII:3xmKate2 time-lapse movies. The time of *de novo* AJ formation was calculated relative to the timing of midbody formation as the timepoint at which Ecad:GFP signal is observed along the whole d-d or n-n interface. The initial AJ length was measured for d-d interface at the time of *de novo* AJ formation.

Junction formation dynamics in the FE

Both Ecad:GFP signal at the *de novo* AJ formed upon cell division and junctional length were determined from time-lapse movies of z-stacks acquired at the surface of Ecad:GFP and MyoII:3xmKate2 egg chambers from control and *rhogef4*$^{\Delta RMCE}$ mutant animals. As the egg chamber curvature prevents the visualization of the whole FE junctional network in individual planes, an adapted projection function (Epitools in Matlab[110]) was used to project the Ecad:GFP and MyoII:3xmKate2 signals from the whole junctional plane into a 2D image. The Ecad:GFP signal at the new cell interface and the interfaces of interphasic cells (used as a reference for normalization) as well as the background signal were manually tracked throughout the time-lapse movie to determine the dynamics of Ecad:GFP fluorescence intensity at the new interface during cell division. To quantify the initial junction length, the length of the newly-formed interface was measured 10 minutes after ring constriction. To take egg chamber curvature into consideration in this analysis, initial junction length was measured using the original z-stacks.

Neighboring membrane withdrawal

The analysis of neighboring cell membrane withdrawal duration was determined at the interface between PH:GFP and PH:mChFP cell patches to distinguish the membranes of the dividing and daughter cell membranes from those of the neighboring cells, focusing on the apical cell level.[36] The duration of neighboring membrane withdrawal was calculated as the difference between the time point of full neighboring membrane insertion and full membrane withdrawal from the dividing cells.

Frequency of rearrangements upon cytokinesis

The analyses of the frequency of n-n AJ formation upon cytokinesis were performed on time-lapse movies of Ecad:GFP in wt and *rhogef4*$^{\Delta RMCE}$ or *rhogef4*$^{\Delta RMCE}$ /Df (3L)BSC117 animals, as well as in ctrl or *rhogef4*$^{\Delta RMCE}$ dividing cells neighboring *cysts* $^{\Delta RMCE}$ clones. The criterion for the formation of a n-n AJ was the formation of a n-n Ecad positive interface for at least one time-point. The formation of n-n AJ occurs either at the time of the initial AJ formation upon cytokinesis, or immediately after the formation of a very short d-d or a 4-fold cell vertex. The formation of n-n AJ formation upon cytokinesis was also observed in *rhogef4*$^{\Delta RMCE}$ clones.

Fluorescent reporter signal levels

MyoII, Ani-RBD and Cysts accumulations in neighboring cells

In control and mutant conditions, the MyoII accumulations in the neighbors were quantified in time-lapse movies of Ecad:GFP and MyoII:3xmKate2 or MyoII:chFP at 80% of constriction of the dividing cell, as previously performed.[42] Upon determination of the time-point corresponding to 80% of the constriction (see above), the accumulation of MyoII:3xmKate2 was quantified as the average of the 2 time points closest to the 80% ring constriction time point. To quantify MyoII:3xmKate2 accumulation in an unbiased manner using Fiji, the mean MyoII:3xmKate2 intensity of the neighboring cells in each frame was used to threshold the image and select the pixels above the mean intensity; thus, defining a ROI corresponding to the MyoII:3xmKate2 accumulation at the base of the ingressing AJ. MyoII accumulation in the neighboring cells was determined as the integrated density of MyoII:3xmKate2 in the ROI normalized by the mean MyoII:3xmKate2 cortical intensity in the neighbors. Note that in Figure 3C, we previously published[42] part of the data used for the graph.

The accumulation of Ani-RBD:GFP in cells neighboring a control dividing cell was analysed in time-lapses movies of His2B-RFP and Ani-RBD:GFP, and visually compared between control and *cysts* neighbors. Ani-RBD:GFP and His2B:RFP are expressed clonally; *cysts* cells are marked by the loss of His2B:RFP signal. Ani-RBD:GFP was analysed in cells adjacent to a cell that divides roughly parallel to them and that is devoid of Ani-RBD:GFP signal.

The localization of Cysts:GFP during cytokinesis was analysed in time-lapse movies of Cysts:GFP together with Ecad:3xmKate2 or MyoII:3xmKate2. To assess the effect of loss of *pnut* knock-down on Cysts accumulation in neighboring cells, the Cysts:GFP signal at the site of AJ deformation by constriction was compared in cells neighboring wt or $pnut^{RNAi}$ (marked by the expression of CAAX:tBFP) dividing cells in Cysts:GFP, Ecad:3xmKate2 time-lapse movies. Using ctrl cells, we first defined that Cysts:GFP accumulation usually begins 3min after the initial deformation of the apical cell junctions due to ring contraction, and it lasts for 4min. Within this time window, we then visually compared Cysts:GFP signal at the ingression site in cells neighboring wt and $pnut^{RNAi}$ dividing cells.

To assess the effect of cytokinetic ring ablation on Cysts accumulation in the neighboring cells, the Cysts:GFP accumulation at the rim of the cytokinetic ring were compared in ablated and non-ablated cytokinetic cells simultaneously imaged within the same field of view.

To assess the effect of *rok* knock-down on Cysts accumulation in the neighboring cells during cytokinesis, the accumulation of Cysts:GFP at the rim of cytokinesis was evaluated in ctrl and rok^{RNAi} (marked by the expression of CAAX:tBFP) neighbors cells surrounding a ctrl dividing cell in Cysts:GFP, MyoII:3xmKate2 time-lapse movies. The accumulation of Cysts:GFP was compared in the rok^{RNAi} neighbors (rok^{RNAi} side) and ctrl cells (ctrl side) surrounding the same dividing cells.

Accumulation of Fluorescent reporters in the contractile ring and daughter cell interface

The analyses of Ani-RBD:GFP, Pak3-RBD:GFP, Scar:GFP, Rac1:GFP and Utr-ABD:GFP signal in the dividing cell were performed on time-lapse movies, together with Ecad:3xmKate2 or MyoII:3xmKate. The mean intensity of each GFP signal was measured at the apical surface level by manually drawing a ROI. The measurements were then averaged over several time-points. The average measurements were corrected by subtracting the averaged cytoplasmic signal in anaphase or cytokinesis. The ROI and timing of measurements were set based on the localization of the GFP and its temporal dynamics: Ani-RBD:GFP was measured at the apical contractile ring starting 2 min after the beginning of cytokinesis (marked by the initial deformation of the apical AJ) and averaged over 6 min (i.e., 3 time-points); Pak3-RBD:GFP and Scar:GFP were quantified at the daughter cell interface starting at the time of midbody formation and averaged over 10 and 6 min (i.e., 5 and 3 time-points), respectively. Rac1:GFP and Utr-ABD:GFP were measured at the daughter cell interface starting at the time of Ecad detachment from contractile ring and averaged over 8 and 10 min (i.e., 4 and 10 time-points), respectively.

Lamin:TagRFP and nls:GFP in telophase daughter cell nuclei

The analysis of Lamin:TagRFP intensity in daughter cell nuclei was performed in time-lapse movies of Lamin:TagRFP and Ecad:GFP. The Lamin:TagRFP intensity was measured at the nuclear envelope upon nuclear reformation during cytokinesis, starting 3 min after the beginning of anaphase during 5 min (i.e., 5 timepoints). To evaluate if nuclear envelope reformation was affected by RhoGEF4 loss of function, we determined nls:GFP reincorporation to the nuclei since defective nuclear sealing reduces nuclear localization of nls:GFP reporter.[111] The analyses were performed in nls:GFP, EcadGFP and MyoII:3xmKate2 time-lapse movies in wt and $rhogef4^{\Delta RMCE}$ conditions. The nls:GFP mean intensity was measured in the cytoplasm and inside the reforming nuclei for 20 min starting from midbody formation. At this time, a weak nls:GFP signal allows to start distinguishing the nuclei. The nuclear/cytoplasmic ratios were then calculated for each cell over time.

Ecad and Cysts colocalization upon LARIAT photoactivation

To evaluate the hypothesis that a decrease in Ecad levels mediated by LARIAT will induce Cysts recruitment, we used notum tissues expressing Ecad:GFP, Cysts:mKate and LARIAT, and photoactivated by blue light illumination. On those tissues, we measured Cysts:mKate and Ecad:GFP levels in junctional regions encompassing Ecad gaps, or in junctional regions without gaps as internal ctrl. For this, we randomly selected each type of region, manually drew a line (1.3-2.6μm length) on each region of interest, and measured the profile of each signal using the Plot profile function in Fiji. For each single line profile of Cysts:mKate-Ecad:GFP, we calculated Spearman correlation coefficients using Graphpad.

Figure preparation

Images were subjected to bleach correction, brightness and contrast modifications and rotation using Fiji. Image denoising was performed using the Fiji despeckle filter, the Gaussian blur Fiji filter, or using a home-made denoising macro in Fiji. When necessary, time-lapse stacks were corrected for apical-basal z-drifts using a custom Fiji macro, or for xy-drifts using the MultistackReg Fiji plugin. For xy views in the notum, all images shown are maximal or sum projections of the relevant z-sections, whereas in yz views all images shown are sum projections of the relevant apical-basal transverse section generated using the Fiji stack reslice tool. As the egg chamber curvature prevents the visualization of the whole FE junctional network in individual planes, an adapted projection function (Epitools in Matlab[110]) was used to project the Ecad:GFP and MyoII:3xmKate2 signals from the whole junctional plane into a 2D image. For FE data, both xy and yz views are maximal projections of the relevant z-sections taken, respectively, at the surface or the midsagittal region of the egg chamber. Kymographs were generated using the multikymograph tool in Fiji.

Graphs were made using GraphPad (Prism). In the box plots, the box extends from the 25th to 75th percentiles (interquartile range), and the line in the middle of the box correspond to the median value. In graphs of any given quantity as a function of time, error bars correspond to the standard error of the mean (SEM).

Sampling and Statistics

Sample sizes vary in each experiment. The experiments were repeated at least two independent times on a minimum of 3 animals. To determine the statistical difference between sets of continuous data, we performed non-parametric Mann-Whitney tests on GraphPad. To determine the statistical difference between two proportions, we performed two-sample Z-score tests for proportions (z-score corresponding to 95% confidence interval = 1.96). For the LARIAT experiment, Spearman coefficients on line measurements of Ecad:GFP and Cysts:mKate2 intensities were calculated using GraphPad.

Significance is indicated by asterisks: *, $p<0.05$; **, $p<0.01$; ***, $p<0.001$; **** and $p \leq 0.0001$.